Self-recovery and fatigue of double-network gels with permanent and reversible bonds

Drozdov, Aleksey D.; Christiansen, Jesper de Claville; Dusunceli, Necmi; Sanporean, Catalina Gabriela

Published in:
Journal of Polymer Science, Part B: Polymer Physics

DOI (link to publication from Publisher):
10.1002/polb.24798

Publication date:
2019

Document Version
Accepted author manuscript, peer reviewed version

Self-recovery and fatigue of double-network gels with permanent and reversible bonds

A.D. Drozdov[1]*, J.deC. Christiansen[1], N. Dusunceli[1,2], C.-G. Sanporean[1]

[1] Department of Materials and Production

Aalborg University, Fibigerstraede 16, Aalborg 9220, Denmark

[2] Department of Mechanical Engineering

Aksaray University, Aksaray 68100, Turkey

Abstract

Double-network (DN) gels subjected to cyclic deformation (stretching up to a fixed strain followed by retraction down to the zero stress) demonstrate a monotonic decrease in strain with time (self-recovery). Observations show that the duration of total recovery varies in a wide interval (from a few minutes to several days depending on composition of the gel), and this time is strongly affected by deformation history. A model is developed for the kinetics of self-recovery. Its ability to describe stress–strain diagrams in cyclic tests with various periods of recovery is confirmed by comparison with observations on several DN gels. Numerical simulation reveals pronounced enhancement of fatigue resistance in multi-cycle tests with stress- and strain-controlled programs when subsequent cycles of deformation are interrupted by intervals of recovery.

Key-words: Double-network gel; Self-recovery; Fatigue; Multi-cycle deformation

1 Introduction

Hydrogels are three-dimensional networks of hydrophilic chains that swell noticeably being immersed into water. As physical properties of gels are similar to those of the extracellular matrix, these materials are widely used in regenerative medicine, tissue engineering and targeted drug delivery [1, 2, 3]. The ability of electroactive gels to conduct electrons [4] and ions [5, 6] opens new

*E–mail: aleksey@m-tech.aau.dk

opportunities for their application in systems for energy conversion and storage: fuel cells, solar cells, Li-ion batteries and supercapacitors [7, 8], wearable and bio-integrated electronic devices [9, 10, 11] and soft hybrid triboelectric nanogenerators [12, 13].

Covalently cross-linked gels are relatively weak and brittle due to the lack of an efficient mechanism for energy dissipation [14]. Strength and toughness of a gel can be enhanced substantially by formation of a double-network (DN) structure [15]. Hydrogels with superior mechanical properties are prepared by introducing reversible bonds between chains able to dissociate and associate under deformation [16]. Design of DN gels (with chains in a permanent network connected by covalent cross-links and chains in a transient network bridged by non-covalent junctions) with high stiffness, strength, toughness, and fatigue resistance has recently become a focus of attention [17, 18]. The following mechanisms are proposed to develop reversible bonds between chains [19]: (i) metal-ligand coordination, (ii) electrostatic interaction (formation of polyion complexes), (iii) hydrogen bonding, (iv) hydrophobic association, and (v) host-guest recognition.

The mechanical behavior of a covalently cross-linked gel is merely elastic. Formation of temporary bonds between chains makes its response viscoelastic and viscoplastic [20]. Viscoelasticity is observed as (i) a strong increase in stress with strain rate in tensile tests and (ii) a substantial decay in stress with time in relaxation tests. Viscoplasticity is observed in cyclic tests as (i) a pronounced difference between the loading and unloading paths and (ii) a strong increase in residual strain (at which stress vanishes under retraction) with maximum strain under stretching. Although the viscoelastic and viscoplastic behavior is revealed not only by gels, but by solid polymers as well [21, 22], the response of DN gels is distinguished by two features: (i) the rate of rearrangement of temporary bonds is comparable with the strain rate in mechanical tests (in relaxation tests on DN gels, stress reaches its minimum value within 2 to 5 min [23, 24], while stress relaxation in solid polymers proceeds for several hours), and (ii) the residual strain after cyclic loading does not remain constant (which is typical of solid polymers [25]), but decays monotonically with time (self-recovery).

The kinetics of self-recovery is conventionally studied in a three-step tensile test (Fig. S1 in Supporting Information): (i) a sample is stretched with a constant strain rate up to some maximum elongation ratio $k_{\max}$ and retracted down to the zero stress with the same strain rate, (ii) the sample is preserved unloaded within some interval of time, and reduction in elongation ratio k is measured as a function of recovery time t_{rec}, (iii) the same cycle of loading-unloading is repeated. The total recovery corresponds to the case when the stress–strain diagram on the recovered specimen coincides

with that on the virgin sample. Observations in recovery tests lead to the following conclusions:

(I) The duration of total recovery varies in a wide interval (from a few minutes to several days) and it depends drastically on the chemical structure of DN gels and preparation conditions (Tab. S1).

(II) The rule of thumb is that the duration of total recovery increases with concentration of covalent cross-links between chains and decreases with concentration of temporary junctions [26]. However, stiffness and strength of bonds affect strongly the rate of recovery. As an example, we refer to observations on poly(acrylamide) (PAAm) copolymer gels covalently cross-linked by N, N'-methylenebisacrylamide (BIS) with various BIS:PAAm ratios r mol.%. For a physically cross-linked PAAm-agar gel ($r = 0$), the duration of total recovery is about 10 min ($k_{\max} = 6$) [27]. This duration exceeds 12 h ($k_{\max} = 10$) for PAAm-gelatin gel with $r = 0.003$ [28] and 24 h ($k_{\max} = 7$) for PAAm-alginate gel with $r = 0.028$ [29]. Surprisingly, total recovery of PAAm gel with $r = 0.1$ physically bonded with tannic acid (TA) can be reached within 5 min ($k_{\max} = 8$) [30].

(III) DN gels able to recover within a few minutes demonstrate an exponential decay [31] in residual strain with recovery time $t_{\rm rec}$. When the recovery process requires more time, it involves two stages [32, 33, 34, 35]: elongation ratio k decreases rapidly with $t_{\rm rec}$ at the first stage, and reduces slowly at the final stage.

(IV) Comparison of observations on as-prepared and fully swollen gel specimens shows that the duration of total recovery is weakly affected by degree of swelling [36].

(V) The growth of maximum elongation ratio under stretching $k_{\max}$ induces an appropriate increase in recovery time [26]. This effect is not, however, pronounced [30].

(VI) The rate of recovery increases with temperature T at which samples are preserved after the first cycle of loading–retraction. When T is below some critical temperature $T_{\rm c}$ at which physical bonds disappear, its effect on the rate of recovery remains modest [28, 29, 37]. At $T > T_{\rm c}$, the time needed for total recovery decays strongly with temperature [38, 39].

The objective of this study is threefold: (i) to develop a model that describes the above features of the self-recovery process, (ii) to find adjustable parameters in the governing equations by fitting observations on a series of DN gels, and (iii) to apply the model in order to predict mutual effects of fatigue and recovery [40, 41] in cyclic tests with stress- and strain-controlled deformation programs.

Numerical simulation focuses on multi-cycle (N cycles with $N \gg 1$) tensile tests on DN gel specimens subjected (along each cycle) to (i) stretching with a constant strain rate up to some elongation ratio $k_{\max}$, (ii) retraction with the same strain rate down to the zero stress $\sigma_{\min} = 0$,

and (iii) recovery (during time $t_{\rm rec}$) at the zero stress. We study (i) the effect of waiting time between subsequent cycles of deformation $t_{\rm rec}$ on the mechanical response of DN gels under fatigue conditions (how the maximum elongation ratio per cycle increases or the maximum stress per cycle decreases with number of cycles) and (ii) the influence of the number of cycles N on the kinetics of self-recovery after termination of cyclic loading. These issues are of essential importance for applications of DN gels in (i) flexible electronic devices (pressure sensors, touch pads [9]) and (ii) regenerative medicine (3D scaffolds for tissue engineering, where cells are subjected to periodic loadings (mechanical cues) interrupted by intervals of rest [42]).

Self-recovery of DN gels was previously studied in [23, 43] by means of the viscoelasticity theory. To explain why durations of the total recovery observed in experiments on DN gels differ by three orders of magnitude, an extension of the model [23, 43] is required, where the influence of viscoplasticity on the kinetics of self-recovery is taken into account. The novelty of our approach consists in (i) modeling the two-stage kinetics of self-recovery within the framework of viscoelasto-plasticity theory with finite strains, and (ii) analysis of interactions between fatigue and recovery in multi-cycle tests with stress- and strain-controlled deformation programs (these interactions have not been considered in previous studies on damage [44, 45] and fatigue of hydrogels [40, 41, 46]).

The ability of the model to describe observations is confirmed by fitting experimental data on (i) poly(vinyl alcohol) (PVA) gel [23, 43], where chains are covalently cross-linked with glutaraldehyde and physically linked with borate ions, (ii) poly(methacrylic acid–*N*-vinyl pyrrolidone–ethylene glycol methyl ether methacrylate) (MAAc-VP-PEGMA) gel [47] with chains connected by hydrogen bonds between MAAc and VP segments, (iii) poly(acrylamide–acrylic acid) (AAm-AAc) gel [48], whose chains are bridged by metal-coordination bonds with Fe^{3+} ions, (iv) poly(acrylamide–acrylic acid–*n*-octadecyl acrylate) (AAm-AAc-ODA) gel [34] physically cross-linked with hydrophobic ODA aggregates and ionic complexes between Fe^{3+} cations and carboxylic groups, and (v) poly(acrylamide–acrylic acid) (AAm-AAc) gel [49], where chains are covalently cross-linked with BIS and physically bonded by Fe^{3+} ions.

2 Model

A DN gel is treated as a two-phase medium composed of an equivalent polymer network and water molecules. The solid and fluid phases are modeled as immiscible interpenetrating continua. Deformation of the network and concentration of water molecules are connected by the molecu-

lar incompressibility condition. An equivalent polymer network in a DN gel is thought of as a superposition of two networks: permanent (where chains are bridged by irreversible covalent cross-links) and transient (where chains are connected by reversible physical bonds). Deformations of the permanent and transient networks coincide with macro-deformation (the affinity hypothesis).

The viscoelastic response of a DN gel is described within the concept of transient networks [50, 51], where chains with sticky ends detach from and attach to temporary junctions being driven by thermal fluctuations. This approach differs from the network alteration theory [52] which accounts for mechanically induced separation of chains from temporary junctions only. To describe inhomogeneity in distribution of temporary bonds with various lifetimes, the transient network is presumed to be composed of meso-regions with various activation energies for detachment [53]. This allows the entire relaxation spectrum of a gel [54, 55, 56] to be expressed in terms of the distribution function for meso-regions [57, 58]. The influence of mechanical factors on the viscoelastic response is taken into account by presuming the attempt rate for detachment of chains to be affected by plastic deformation. The rate of merging of dangling chains with the network is determined from the conservation law for concentration of active chains. Alternative approaches to modeling the kinetics of separation of chains from temporary bonds and their attachment to the transient network were proposed in [54, 55, 60, 61, 62, 63].

The viscoplastic response of a DN gel is treated as sliding of junctions in the permanent network with respect to their initial positions [64]. A junction starts to slide when one of the chains connected by this junction is transformed from the active state into the dangling state (which means that stress in this chain vanishes suddenly). Plastic flow proceeds until the junction reaches a new equilibrium state. The rate of plastic deformation is governed by dissipation of energy of inter-chain interaction in the permanent network.

Constitutive equations for the kinetics of self-recovery and the viscoelastic and viscoplastic responses of a DN gel under arbitrary three-dimensional deformation with finite strains are derived in Supporting Information from the free energy imbalance inequality by using a method proposed in [65]. For a swollen gel equilibrated before loading and subjected to uniaxial tensile cyclic deformation, the governing equations involve

(i) The formula for engineering tensile stress

$$\sigma = G\Big[(1-\kappa)\frac{k^3-k_{\rm p}^3}{k^2k_{\rm p}^2}+\kappa\Big(S_1k-\frac{S_2}{k^2}\Big)\Big], \tag{1}$$

where k and $k_{\rm p}$ are elongation ratios for macro-deformation and plastic deformation, respectively.

(ii) The integral relations for the functions S_1 and S_2 that describe the response of the transient network

$$S_1 = \int_0^\infty f(u)s_1(t,u)\mathrm{d}u, \qquad S_2 = \int_0^\infty f(u)s_2(t,u)\mathrm{d}u, \tag{2}$$

where

$$f(u) = f_0 \exp\Big(-\frac{u^2}{2\Sigma^2}\Big) \qquad (u \geq 0) \tag{3}$$

stands for the distribution function of meso-regions with various dimensionless activation energies u, $\Sigma > 0$ is a material constant, and the coefficient f_0 is determined from the normalization condition $\int_0^\infty f(u)\mathrm{d}u = 1$.

(iii) The kinetic equations for the functions s_1 and s_2

$$\frac{\partial s_1}{\partial t} = \Gamma\Big(\frac{1}{k^2} - s_1\Big), \qquad \frac{\partial s_2}{\partial t} = \Gamma(k - s_2), \qquad s_1(0,u) = s_2(0,u) = 1, \tag{4}$$

where

$$\Gamma = \bar{\gamma}\exp(-u) \tag{5}$$

is the rate of separation of chains from temporary junctions, and $\bar{\gamma} > 0$ is the attempt rate.

(iv) The kinetic equation for plastic flow

$$\dot{k}_\mathrm{p} = P\Big[\frac{k^3 - k_\mathrm{p}^3}{kk_\mathrm{p}} - R(k_\mathrm{p}^3 - 1)\Big], \qquad k_\mathrm{p}(0) = 1. \tag{6}$$

(v) The kinematic equation for elongation ratio k_e for elastic deformation

$$k_\mathrm{e} = \frac{k}{k_\mathrm{p}}. \tag{7}$$

Under stretching–retraction with a constant strain rate $\dot{\epsilon}$, these relations are accompanied by the kinematic equation for elongation ratio k under macro-deformation

$$\dot{k} = \pm\dot{\epsilon}, \qquad k(0) = 1, \tag{8}$$

where the signs "+" and "–" correspond to loading and unloading, respectively.

For self-recovery of a DN gel under the zero stress, Eqs. (2)–(7) remain unchanged, whereas Eqs. (1) and (8) are replaced with the nonlinear equation

$$k = \left(\frac{k_\mathrm{p} + \kappa_1 S_2}{k_\mathrm{p}^{-2} + \kappa_1 S_1}\right)^{\frac{1}{3}}, \qquad \kappa_1 = \frac{\kappa}{1-\kappa}. \tag{9}$$

Eqs. (1)–(9) involve three material constants: G, κ and Σ. The governing equations contain also three adjustable functions: $\bar{\gamma}$, P and R.

The coefficient $\bar{\gamma}$ stands for the attempt rate for detachment of chains from temporary junctions. This quantity is presumed to be affected by evolution of the structure of the equivalent polymer network (reflected by sliding of permanent junctions with respect to their reference positions). The following dependence is adopted:

$$\bar{\gamma} = \gamma \exp[-\alpha(I_{\mathrm{p}2} - 3)], \tag{10}$$

where γ is the attempt rate at infinitesimal strains, the exponent α describes the influence of plastic flow on the rate of rearrangement, and $I_{\mathrm{p}2} = 2k_{\mathrm{p}} + k_{\mathrm{p}}^{-2}$ stands for the second principal invariant of the Cauchy–Green tensor for plastic deformation. For a positive α, Eq. (10) is equivalent, in some sense, to the time–stress superposition principle in nonlinear viscoelasticity [66]. It follows from this relation that under retraction, when stress σ decreases and k_{p} increases, the growth of k_{p} results in a decay in the relaxation rate, whereas under reloading, when σ grows and k_{p} is reduced, the decrease in k_{p} induces an increase in $\bar{\gamma}$.

The coefficient P stands for the rate of sliding of permanent junctions with respect to their reference positions, and the coefficient R denotes the ratio of moduli G_{p} and G_{e} that characterize mechanical energies dissipated and stored in the permanent network.

In the analysis of multi-cycle loading interrupted by recovery, four regimes of deformation are distinguished: (i) stretching of a virgin sample ($\dot{k} > 0$, $\dot{\sigma} > 0$), (ii) retraction ($\dot{k} < 0$, $\dot{\sigma} < 0$), (iii) recovery ($\dot{k} < 0$, $\dot{\sigma} = 0$), and (iv) reloading ($\dot{k} > 0$, $\dot{\sigma} > 0$). We presume the parameter P to vanish under stretching, and to adopt different values, P_1, P_2, P_3, under retraction, recovery, and reloading:

$$P = 0 \quad \text{(stretching)}, \quad P = P_1 \quad \text{(retraction)}, \quad P = P_2 \quad \text{(recovery)}, \quad P = P_3 \quad \text{(reloading)}. \tag{11}$$

To describe stress-induced acceleration of plastic flow under retraction, we denote by p_1 the rate of sliding of junctions at the instant when unloading starts and tensile stress reaches its maximum value $\sigma_{\max}$, and set

$$P_1 = p_1 \exp[\beta_1(\sigma_{\max} - \sigma)], \tag{12}$$

where σ stands for tensile stress at an arbitrary instant t, and β_1 is a constant exponent.

The kinetics of plastic deformation under recovery of a DN gel reflects evolution of its microstructure. To describe this evolution, we introduce the relative plastic elongation ratio

$$k_{\mathrm{r}} = \frac{k_{\mathrm{p}0}}{k_{\mathrm{p}}},$$

where $k_{\rm p0}$ and $k_{\rm p}$ stand for elongation ratios for plastic deformation at the instant t_0, when recovery starts, and an arbitrary instant $t > t_0$, denote by $I_{\rm r2} = 2k_{\rm r} + k_{\rm r}^{-2}$ the second principal invariant of the corresponding Cauchy–Green tensor, and postulate that

$$P_2 = p_2 \exp[-\beta_2(I_{\rm r2} - 3)], \tag{13}$$

where p_2 is the rate of sliding of junctions at the beginning of recovery, and β_2 is a constant coefficient.

Sliding of junctions under reloading is affected by interplay between (i) tensile stress and (ii) evolution of the structure of polymer network. To account for the cooperative effect of these factors, we introduce some threshold stress $\bar{\sigma}$, and presume the rate of plastic flow P_3 to remain constant at $\sigma < \bar{\sigma}$ and to increase with stress at $\sigma > \bar{\sigma}$:

$$\begin{aligned} P_3 &= p_3 \qquad (\sigma < \bar{\sigma}), \\ P_3 &= p_3[1 + \beta_3(\sigma - \bar{\sigma})^2], \qquad (\sigma \geq \bar{\sigma}). \end{aligned} \tag{14}$$

Here p_3 is the rate of sliding of junctions at the beginning of reloading, and β_3 characterizes changes in the structure of polymer network under retraction and subsequent recovery. In treatment of observations, the threshold stress $\bar{\sigma}$ corresponds to the inflection point on the reloading path when reloading starts immediately after retraction: this curve is convex at $\sigma < \bar{\sigma}$ and concave at $\sigma > \bar{\sigma}$.

By analogy with Eq. (11), the coefficient R is presumed to accept different values under retraction, recovery, and reloading

$$R = R_1 \quad \text{(retraction)}, \qquad R = R_2 \quad \text{(recovery)}, \qquad R = R_3 \quad \text{(reloading)}. \tag{15}$$

The constitutive model consists of three parts: (i) stress–strain equations (1)–(8) for the viscoelastic and viscoplastic behavior of a DN gel under cyclic deformation, (ii) Eq. (9) for its mechanical response under recovery, and (iii) semi-phenomenological relations (10)–(15) for the parameters $\bar{\gamma}$ (reflecting the viscoelastic response) and P_m, R_m (describing the kinetics of plastic flow).

The difference between Eqs. (1)–(8) and the governing equations in viscoelastoplasticity of DN gels proposed in our previous studies consists in the following: (i) unlike [59], the transient network is presumed to be inhomogeneous and composed of meso-regions with various activation energies for breakage of temporary bonds, (ii) contrary to [59, 67], the strain energy density of the permanent network is adopted in the neo-Hookean form, and the only mechanism of plastic flow

(due to inter-chain interaction) is taken into account. These simplifications allow Eqs. (1) and (6) to be presented in the novel form convenient for numerical simulation, and an explicit expression to be derived for elongation ratio under self-recovery, see Eq. (9), which serves as one of the main results of this work.

Nonlinear dependencies (10)–(15) are introduced to describe mutual effects of rearrangement of temporary bonds in the transient network and sliding of junctions in the permanent network. In particular, we take into account (i) the effect of plastic flow on the rate of separation of chains from temporary bonds, Eq. (10), (ii) the influence of plastic deformation on the rate of recovery, Eq. (13), and (iii) the effects of stress on the rates of plastic flow under retraction, Eq. (12), and reloading, Eq. (14).

The governing equations involve 15 material constants: (i) G stands for the elastic modulus of a gel, (ii) κ is the ratio of the elastic modulus of the transient network to that of the gel, (iii) Σ is a measure of inhomogeneity of the transient network, (iv) γ is the attempt rate for separation of chains from temporary bonds, (v) α accounts for the effect of plastic deformation on the attempt rate, (vi) $\bar{\sigma}$ stands for the threshold stress on the reloading path of the stress–strain diagram, and (vii) P_m, R_m and β_m describe sliding of junctions in the permanent network under retraction ($m = 1$), recovery ($m = 2$), and reloading ($m = 3$). Although the number of adjustable parameters is not small, this number is comparable with that in other models for the viscoelastic and viscoplastic responses of polymers under multi-cycle deformation.

3 Fitting of observations

The ability of the constitutive model to describe experimental stress–strain diagrams in cyclic (loading–unloading) tests with various maximum elongation ratios $k_{\max}$ and recovery (stretching-retraction-recovery-reloading-unloading) tests with various durations of recovery $t_{\rm rec}$ is examined on a series of DN gels with covalent and non-covalent bonds.

It is worth noting that the experimental protocol in conventional recovery tests differs slightly from that described in Introduction. To avoid evaporation of water under recovery, a gel sample is unloaded down not to the zero stress ($\sigma = 0$), but to its initial length ($k = 1$), taken from the testing machine, preserved during a fixed interval of time being wrapped with a plastic film, reinstalled into the testing machine, and reloaded from $k = 1$ (not from the elongation ratio reached at the end of self-recovery process). Retraction down to the initial length of a sample leads to its buckling

under negative (compressive) stress and damage accumulation [23]. As this damage is restored under reloading only partially, the very initial intervals of the reloading paths are disregarded in the fitting procedure. The same procedure (retraction down to $k = 1$ and reloading of the buckled specimen) is used to analyze the response of gels under "immediate" reloading. In this case, $t_{\rm rec}$ is calculated as the time necessary for compression (from the k value corresponding to $\sigma = 0$ to $k = 1$) and tension (from $k = 1$ to the elongation ratio as which σ starts to grow under reloading).

3.1 PVA gel

We begin with the analysis of observations [23] on PVA gel synthesized by means of a two-stage procedure. At the first stage, PVA chains in an aqueous solution (12 wt.%, molecular weight 89 to 98 kg/mol) were covalently cross-linked with glutaraldehyde (molar fraction 5.5 mM). The swollen gel was immersed into an aqueous solution of sodium tetraborate decahydrate (1 mM) and sodium chloride (90 mM) for 3 days. The permanent network is formed by chains bridged by chemical cross-links. In the transient network, chains are linked by physical bonds between hydroxyl groups of PVA and borate ions.

Mechanical tests were conducted on as-prepared specimens with degree of swelling $Q = 8.3$. The experimental program involves: (i) cyclic test with strain rate $\dot\epsilon = 0.03$ s^{-1} and maximum elongation ratio $k_{\rm max} = 2$, and (ii) relaxation test with strain rate under stretching $\dot\epsilon = 0.2$ s^{-1} and elongation ratio $k_{\rm max} = 1.1$. Observations in these tests are reported in Fig. 1 together with results of simulation with the material constants listed in Tab. S2. Tensile stress σ is plotted versus elongation ratio k in Fig. 1A. The stress σ is depicted versus relaxation time $t_{\rm rel}$ in Fig. 1B.

Adjustable parameters are determined by means of an iterative algorithm. We start with fixing the triplet (γ, κ, Σ), and determine G from the best-fit condition for the stress–strain diagram under tension in Fig. 1A. Then, we fix G, and find parameters γ, κ, Σ that ensure the best fit of the corresponding relaxation curve in Fig. 1B. Taking these parameters as a new approximation for the triplet (γ, κ, Σ), we return to approximation of the stress–strain curve under stretching in Fig. 1A. Simulation shows that three iterations are sufficient to ensure good agreement between the data in Figs. 1A and 1B and the results of numerical analysis. Experimental data under retraction (Fig. 1A) are not used in the fitting procedure (we suppose that plastic flow is absent in the gel).

To examine the ability of the model to predict the response of DN gels, simulation is conducted of recovery tests on PVA gel with various durations of recovery $t_{\rm rec} = 5$ s, 10 s, 1 min, 2 min and 5 min. Results of numerical analysis are reported in Fig. 1C, which shows that after 5 min of

recovery, the stress–strain diagram along the second cycle of deformation coincides practically with that for the virgin specimen (in accord with experimental data). The decay in elongation ratio k with recovery time $t_{\rm rec}$ is illustrated in Fig. 1D. According to this figure, PVA gel with the merely viscoelastic response (all rates of plastic flow P_m vanish) demonstrates an exponential kinetics of recovery.

3.2 MAAc-VP-PEGMA copolymer gel

We fit experimental data [47] on poly(methacrylic acid–*N*-vinyl pyrrolidone–ethylene glycol methyl ether methacrylate) (MAAc-VP-PEGMA) copolymer gel. The gel was prepared by photo-polymerization of the pre-gel solution (MAAc and VP monomers were mixed with an aqueous solution of PEGMA chains with weight fractions 150.6 g/L, 194.5 g/L, and 103.5 g/L, respectively) by using Irgacure 2959 (0.5 mol.% with respect to monomers) as a photo-initiator. Chains in the permanent network are linked by entanglements and hydrogen bonds between carboxylic groups (MAAc) and carbonyl groups (VP) whose lifetime exceeds the duration of tests, whereas chains in the transient network are bridged by hydrogen bonds between carboxylic and carbonyl groups with short lifetimes and by ionic complexes between partially ionized anionic and cationic groups [68, 69].

Mechanical tests were performed at room temperature on fully swollen samples with degree of swelling $Q = 5.2$. The experimental program involves: (i) a series of cyclic tests with strain rate $\dot\epsilon = 0.154$ s^{-1} and various maximum elongation ratios $k_{\rm max}$ ranging from 1.5 to 4.0, (ii) cyclic test with the same strain rate and maximum elongation ratio $k_{\rm max} = 6$, (iii) a series of recovery tests with strain rate $\dot\epsilon = 0.154$ s^{-1}, maximum elongation ratio $k_{\rm max} = 3$, and various durations of recovery $t_{\rm rec}$ randing from 30 s to 15 min, (iv) total recovery test with the same strain rate, maximum elongation ratio $k_{\rm max} = 6$, and duration of recovery $t_{\rm rec} = 30$ min. Observations in these tests are reported in Fig. 2 together with results of numerical analysis with the material constants collected in Tab. S3. Tensile stress σ is plotted versus elongation ratio k in Figs. 2A to 2D. Elongation ratio k is depicted versus recovery time $t_{\rm rec}$ in Figs. 2E and 2F.

Adjustable parameters are determined by means of the following algorithm. Bearing in mind that observations in relaxation tests are not provided, the coefficients G, γ, κ, Σ are found from the best-fit condition for the stress-strain diagrams under stretching in Fig. 2A and 2B. As the loading paths in these figures differ from one another, material constants are determined separately.

Then, we set $\alpha = 0$ (no effect of plastic deformation on the rate of separation of chains from temporary junctions) and $\beta_1 = 0$ (no influence of stress on the rate of plastic flow) and match

each retraction path in Fig. 2A by means of two parameters, p_1 and R_1. The effect of elongation ratio $k_{\max}$, at which unloading starts, on these quantities is illustrated in Fig. S2A. Evolution of p_1 and R_1 with $k_{\max}$ (that reflects damage accumulation (changes in the micro-structure of a DN gel) under multi-cycle deformation) is described by the equations

$$\log p_1 = p_1^0 + p_1^1(I_{e2} - 3), \qquad \log R_1 = R_1^0 + R_1^1(I_{e2} - 3), \tag{16}$$

where $\log = \log_{10}$, the second principal invariant of the Cauchy–Green tensor for elastic deformation $I_{e2} = 2k_e + k_e^{-2}$ is calculated at the point where the strain rate $\dot{\epsilon}$ changes its sign, and the coefficients are found by the least-squares technique.

The same procedure is applied to match observations in Fig. 2B. The only difference is that the stress–strain diagram under retraction is approximated with the help of 3 parameters, p_1, R_1, and α (the latter is given in Tab. S3). The coefficients p_1 and R_1 are reported in Fig. S2A.

For each recovery time $t_{\rm rec}$, the elongation ratio k at which reloading starts is determined from Fig. 2C. The data are depicted in Fig. 2E together with their fit by the model with the coefficients p_2, R_2 and β_2 found from the best-fit condition. For observations in Fig. 2D, the same values of p_2 and R_2 are used, while the coefficient β_2 is determined from the condition of total recovery within 30 min, see Fig. 2F.

Reloading paths of the stress–strain curves in Fig. 2C are matched by presuming $\bar{\sigma} = 0$. We start with observations at $t_{\rm rec} = 30$ s and determine p_3, R_3 and β_3 from the best-fit condition for the corresponding reloading diagram. Then, we fix p_3 and R_3 and approximate the other reloading curves by using the only parameter β_3. The effect of plastic deformation on this quantity is illustrated in Fig. S2B. The data are approximated by the equation

$$\log \beta_3 = \beta_3^0 + \beta_3^1 \sqrt{\bar{I}_{p2} - 3}, \tag{17}$$

where $\bar{I}_{p2}$ stands for the second principal invariant of the Cauchy–Green tensor for plastic deformation $I_{p2} = 2k_p + k_p^{-2}$ calculated at the point with $\sigma = \bar{\sigma}$, and the coefficients are determined by the least-squares method.

Prediction of the stress–strain diagrams along the second retraction paths in Figs. 2C and 2D is performed with the coefficients p_1, R_1 and β_1 determined by fitting observations along the first retraction.

3.3 AAm-AAc gels

Observations are analyzed on poly(acrylamide–acrylic acid) (AAm-AAc) copolymer gels with chains connected by metal-coordination bonds between mobile Fe^{3+} cations and fixed carboxylic groups. To evaluate the effect of other covalent and non-covalent junctions between chains on the kinetics of self-recovery, three types of gels are studied: (i) where chains are connected by ionic complexes only, (ii) where hydrophobic aggregates are introduced into the network as non-covalent links, and (iii) where chains are chemically cross-linked. Material constants in the governing equations are determined by using the algorithm exposed in Section 3.2.

We begin with fitting experimental data [48] on AAm-AAc gel, whose chains are linked by metal-coordination bonds only. The gel was prepared by free radical polymerization of a precursor solution of AAm (17 wt.%) and AAc (3 wt.%) monomers in deionized water by using potassium persulfate (KPS, 0.2 wt.%) as an initiator. The copolymer solution was precipitated in acetone, redissolved in water, and dried. The samples were immersed into an aqueous solution of iron chloride hexahydrate $FeCl_3 \cdot 6H_2O$ (100 mM) for 8 h and swollen in deionized water for 24 h. The permanent network is formed by chains bridged by entanglements and metal-coordination bonds whose lifetime exceeds the duration of tests. Chains in the transient network are connected by physical junctions whose lifetime is comparable with this duration.

Experiments were conducted on fully swollen specimens with an unspecified degree of swelling. In each test, a sample was stretched with strain rate $\dot{\epsilon} = 0.139$ s^{-1} up to the maximum elongation ratio $k_{\max} = 3.5$ and retracted with the same strain rate down to the zero stress. Afterwards, the sample was preserved unloaded for various recovery times $t_{\rm rec}$ ranging from 2 min to 4 h. Finally, the second cycle of loading–unloading was performed with the same strain rate and maximum elongation ratio. Experimental data in these tests are depicted in Fig. 3 together with results of simulation with the material constants listed in Tab. S4. Tensile stress σ is plotted versus elongation ratio k in Fig. 3A. The decay in elongation ratio k with recovery time $t_{\rm rec}$ is reported in Fig. 3B.

Each reloading path of the stress–strain diagrams in Fig. 3A is determined by the only coefficient β_3. Unlike the MAAc-VP-PEGMA gel, whose β_3 grows exponentially with elongation ratio for plastic deformation (Fig. S2B), observations on AAm-AAc gel show that this parameter remains constant $\beta_3 = 0.52$ at sufficiently large recovery times, $t_{\rm rec} \geq 15$ min. An increase in β_3 is observed at small durations of recovery only: $\beta_3 = 2.4$ at $t_{\rm rec} = 2$ min.

To ensure good agreement with observations along the second unloading path, the coefficients

p_1 and R_1 are treated as adjustable parameters. The effect of recovery time on these quantities is illustrated in Fig. S3, where the data are approximated by the equations

$$\log p_1 = p_1^0 + p_1^1 \log t_{\rm rec}, \qquad \log R_1 = R_1^0 + R_1^1 \log t_{\rm rec} \tag{18}$$

with coefficients calculated by the least-squares method.

We proceed with matching observations [34] on poly(acrylamide–acrylic acid–*n*-octadecyl acrylate) (AAm-AAc-ODA) gel. First, micellar copolymerization was conducted of AAm monomers (12 wt.%), AAc monomers (10 wt.% of AAm) and ODA monomers (35 wt.% of AAm) in an aqueous solution of sodium dodecyl sulfate (SDS, 18 wt.%) and sodium chloride (1.5 M) by using ammonium persulfate (APS, 1 wt.%) as an initiator. Afterwards, the gel was soaked in distilled water at room temperature to extract SDS and residual monomers. The samples were immersed in an aqueous solution of iron chloride hexahydrate $FeCl_3 \cdot 6H_2O$ (50 mM) for 24 h and rinsed in deionized water for 48 h. The permanent network is formed by chains linked by hydrophobic aggregates of ODA, while chains in the transient network are bonded by ionic complexes between Fe^{3+} cations and fixed carboxyl groups.

Mechanical tests were conducted on fully swollen specimens with degree of swelling $Q = 2.6$ by using the same protocol as for AAm-AAc gel. The only difference is that experiments were performed with the strain rate $\dot\epsilon = 0.083$ s^{-1} and maximum elongation ratio equals $k_{\max} = 2.5$. Observations are depicted in Fig. 4 together with results of simulation with the material constants listed in Tab. S5. Tensile stress σ is plotted versus elongation ratio k in Fig. 4A. The decay in elongation ratio k with recovery time $t_{\rm rec}$ is reported in Fig. 4B.

Each stress–strain diagram under reloading in Fig. 4A is determined by the only parameter β_3. Evolution of this quantity with plastic deformation is illustrated in Fig. S4, where the data are approximated by Eq. (17). Fig. 4A reveals an acceptable agreement between experimental data and results of numerical analysis when the same coefficients p_1 and R_1 are used in simulation of the first and second unloading paths.

Finally, we fit observations [49] on double cross-linked AAm-AAc gel. Free-radical cross-linking polymerization of AAm and AAc monomers was performed in an aqueous solution (molar fraction of AAm 90 mM; AAc:AAm molar ratio 0.15) by using BIS as a cross-linked (0.0216 mol.% with respect to monomers), KPS as an initiator (1 wt.%), and N, N, N', N'-tetramethyldiamine (TEMED) as an accelerator (0.0083 wt.%). The gel was soaked in an aqueous solution of iron chloride hexahydrate (4.05 g in 250 mL of water) for 16 h and swollen in deionized water for 48 h. Chains in the

permanent network are covalently cross-linked by BIS, while chains in the transient network are bonded by ionic complexes between Fe^{3+} cations and fixed carboxyl groups.

Mechanical tests were conducted at room temperature on as-prepared samples with an unspecified degree of swelling. The program involves: (i) a series of cyclic tests with strain rate $\dot{\epsilon} = 0.083$ s^{-1} and maximum elongation ratios k_{max} ranging from 2 to 6, and (ii) a series of recovery tests (loading–unloading with strain rate $\dot{\epsilon} = 0.083$ s^{-1} and maximum elongation ratio $k_{max} = 4$ followed by recovery at the zero stress and subsequent loading–unloading with the same strain rate and maximum elongation ratio) with various recovery times t_{rec} ranging from 30 s to 4 h. Experimental data are depicted in Fig. 5 together with results of simulation with the material constants collected in Tab. S6. Stress–strain diagrams under loading-unloading with various k_{max} are presented in Fig. 5A. Tensile stress σ in recovery tests is plotted versus elongation ratio k in Fig. 5B. The decay in elongation ratio k with recovery time t_{rec} is shown in Fig. 5C. Bearing in mind that the stress–strain curves under tension in Figs. 5A and 5B differ noticeably, the data reported in these figures are matched separately.

Each retraction path of the stress–strain diagrams in Fig. 5A is characterized by the only coefficient p_1. The effect of k_{max} on this quantity is demonstrated in Fig. S5A where the data are approximated by Eq. (16). Each reloading path of stress–strain curves Fig. 5B is determined by the only coefficient β_3. Evolution of this parameter with plastic deformation is shown in Fig. S5B, where the data are approximated by Eq. (17). To ensure good agreement with observations along the second unloading paths on the stress–strain diagrams presented in Fig. 5B, the coefficients p_1 and R_1 are treated as adjustable parameters. The effect of recovery time t_{rec} on these quantities is illustrated in Fig. S5C, where the data are approximated by Eq. (18).

Comparison of material parameters in Tabs. S4 to S6 leads to the following conclusions:

(I) The elastic modulus G of AAm-AAc gel with metal-coordination bonds exceeds those for AAm-AAc gels with extra non-covalent and covalent cross-links by factors of two and four. This may be explained by (i) a larger mass fraction of AAc monomers in the polymer network (0.18 compared with 0.10 and 0.15) and a higher concentration of Fe^{3+} ions under soaking.

(II) The stiffnesses of the transient network κ adopts similar values for all three hydrogels.

(III) The attempt rates for detachment of chains from temporary junctions γ adopt similar values for physical AAm–AAc and AAm-AAc-ODA gels. These values exceed the attempt rate for the double cross-linked gel, which means that rearrangement of the transient network is strongly decelerated by the presence of covalent cross-links.

(IV) The presence of extra junctions in a network of chains connected by metal-coordination bonds causes its homogenization (a decrease in Σ).

(V) The parameters reflecting plastic flow under retraction adopt similar values for all three gels.

(VI) The coefficients responsible for the recovery process are similar for physically cross-linked and double cross-linked AAm-AAc gels. Their rates of recovery exceed strongly (by an order of magnitude) that for AAm-AAc-ODA gel (characterized by a small rate of plastic flow under recovery p_2 and a large coefficient of its deceleration β_2). The latter is confirmed by observations showing that the same degree of recovery is reached after 4 h in AAm-AAc gels stretched up to 250 and 300% as in AAm-AAc-ODA gel stretched up to 150% only (Figs. 3B, 4B, 5C).

(VII) The influence of recovery time $t_{\rm rec}$ on coefficients p_1, R_1 and β_1 appears to be of secondary importance. Fig. 4A demonstrates rather weak deviations between the first and second retraction paths when this effect is disregarded.

3.4 Discussion

Figs. 1 to 5 confirm the ability of the model to describe experimental stress–strain diagrams in relaxation tests, cyclic tests with various maximum elongation ratios, and recovery tests with various durations (weak deviations are to be noticed between the observations in Figs. 3A and 5A and results of simulation for large $t_{\rm rec}$).

Figs. S2 to S5 show that adjustable parameters in the governing equations evolve consistently with experimental conditions (maximum strain per cycle and duration of self-recovery).

The main difference between the observations reported in Fig. 1 and those depicted in Figs. 2 to 5 consists in the fact that the mechanical behavior of PVA gel is merely viscoelastic, whereas the responses of the other gels show combinations of the viscoelastic and viscoplastic features. This explains also why the number of constants reported in Tab. S2 (all P_m vanish for this material) is essentially lower that that in Tabs. S3–S6.

To demonstrate that the viscoelastic response of PVA gel is not exceptional, experimental data [70] are fitted on supramolecular polydimethylsiloxane (PDMS) elastomer. In this material, bipyridine (2,2′-bipyridine-5,5′-dicarboxylic amide) was incorporated into the backbone of PDMS chains. Chains in the permanent network are linked by entanglements whose lifetime exceeds the duration of tests. Chains in the transient network are bridged by metal-ligand coordination bonds between Fe^{2+} ions and bipyridine moieties.

Mechanical tests were performed at room temperature. The experimental program involves (i) cyclic test with strain rate $\dot{\epsilon} = 0.0167$ s^{-1} and maximum elongation ratio $k_{\max} = 2$, and (ii) relaxation test with the same rate under stretching and elongation ratio $k = 1.03$. Observations are depicted in Fig. 6 together with results of simulation with the material constants collected in Tab. S7. The Young's modulus $E = 3G$ calculated by matching the entire stress–strain diagram in Fig. S6A ($E = 1.02$ MPa) is in accord with $E = 0.9 \pm 0.2$ MPa found by fitting observations under stretching with small strains [70].

Comparison of Tabs. S2 and S7 implies that the rate of rearrangement of temporary bonds γ in the PVA gel exceeds that in PDMS elastomer by an order of magnitude (the rearrangement process is strongly accelerated by the presence of water), while the inhomogeneity of the temporary network in the elastomer Σ is noticeably higher than that in the gel (which may be explained by the presence of several mechanisms for metal-ligand coordination [70]).

Experimental data show that the coefficient β_3 (that describes stress-strain curves under reloading of recovered samples) increases with plastic elongation ratio $k_{\rm p}$ (this quantity is inversely proportional to $t_{\rm rec}$) for MAAc-VP-PEGMA gel [47] and AAm–AAc gels [34, 48] and decreases with this parameter (at large recovery times) for double cross-linked AAm–AAc gel [49]. As the accuracy of observations appears to be insufficient to discriminate between these two types of response (under recovery for long times, water evaporation is unavailable even when samples are wrapped with plastic films), simulation is conducted to reveal which consequences are expected by presuming β_3 to increase and decrease with $k_{\rm p}$. Numerical analysis is performed for Mullins-type tests interrupted by self-recovery (stretching up to elongation ratio $k_{\max 1}$, retraction down to the zero stress, recovery for time $t_{\rm rec}$, reloading up to elongation ratio $k_{\max 2} > k_{\max 1}$, and unloading down to the zero stress) on MAAc-VP-PEGMA gel whose material constants are collected in Tab. S3 and double cross-linked AAm–AAc gel whose parameters are listed in Tab. S6. Results of simulation are depicted in Figs. S6 and S7. These figures demonstrate a monotonic increase in tensile stress under reloading with recovery time $t_{\rm rec}$ for AAm-AAc gel (β_3 decreases) and non-monotonic changes in stress (in the interval between $k_{\max 1}$ and $k_{\max 2}$) with $t_{\rm rec}$ for MAAc-VP-PEGMA gel (β_3 increases). Based on these observations, it seems reasonable to presume β_3 to evolve with $t_{\rm rec}$ non-monotonically: this parameter decreases with $t_{\rm rec}$ at small recovery times, reaches its minimum, and increases at large durations of recovery. To validate this hypothesis, observations are needed in recovery tests with small durations (in the interval from 1 to 5 min).

4 Predictions of the model

As recovery of elastomers (covalently cross-linked networks) is negligible, their fatigue resistance is conventionally studied in multi-cycle loading–unloading tests without waiting periods between cycles. Although the response of polymer networks with covalent and non-covalent bonds in fatigue tests is strongly influenced by recovery [41], only a few experimental studies have focused on this effect. Comparison of the stress–strain diagrams on virgin and recovered specimens (total recovery for 24 h after a deformation cycle) in multi-cycle tests is conducted in [71, 72, 73]. Observations in a multi-cycle test with a fixed (5 min) interval of recovery between cycles are reported in [35]. The above studies dealt with the response of DN gels in cyclic tests with a strain-controlled (a fixed maximum elongation ratio per cycle $k_{\max}$) programs and relatively small (below 10) numbers of cycles.

Our aim is to evaluate (by means of simulation) the effect of recovery time between cycles $t^{\mathrm{c}}_{\mathrm{rec}}$ on the response of DN gels in tests with strain-controlled (fixed maximum elongation ratio per cycle $k_{\max}$) and stress-controlled (fixed maximum stress per cycle $\sigma_{\max}$) programs and relatively large numbers of cycles (N of order of 10^3), on the one hand, and to assess how the number of cycles N affects the kinetics of self-recovery after multi-cycle deformation, on the other.

We begin with the analysis of PVA gel with material constants collected in Tab. S2. Simulation is conducted for multi-cycle ($N = 50$) tests with a strain-controlled program ($k_{\max} = 2$) and various durations of recovery between cycles $t^{\mathrm{c}}_{\mathrm{rec}}$ ranging from 1 s to 1 min. The stress–strain diagrams are depicted in Fig. S8, and the maximum stress per cycle $\sigma_{\max}$ is plotted versus number of cycles n in Fig 7. The following conclusions are drawn:

(I) The hysteresis energy (estimated as the area between subsequent loading–retraction paths) increases strongly with $t^{\mathrm{c}}_{\mathrm{rec}}$.

(II) The maximum stress per cycle $\sigma_{\max}$ is reduced with number of cycles n. The decrease in $\sigma_{\max}$ is substantial along the first few cycles, and becomes weak (linear in n) afterwards.

(III) Changes in $\sigma_{\max}(n)$ are decelerated substantially with the growth of recovery time between cycles $t^{\mathrm{c}}_{\mathrm{rec}}$.

Results of numerical analysis for multi-cycle tests with a stress-controlled program and various durations of recovery between cycles are presented in Figs. 8 and S9. For tests with $N = 50$ cycles, $\sigma_{\max} = 5$ kPa, and various $t^{\mathrm{c}}_{\mathrm{rec}}$, the stress σ is plotted versus elongation ratio k in Fig. S9, and the maximum elongation ratio per cycle $k_{\max}$ is depicted versus number of cycles n in Fig. 8A. For tests with $N = 1000$ cycles, $t^{\mathrm{c}}_{\mathrm{rec}} = 1$ s, and various maximum stresses $\sigma_{\max}$, evolution of $k_{\max}$ with

number of cycles n is demonstrated in Fig. 8B. These figures reveal that

(I) The maximum elongation ratio per cycle $k_{\max}$ increases with number of cycles n. The growth of $k_{\max}$ is strong during the first few cycles (primary fatigue), and becomes linear in n (secondary fatigue) afterwards.

(II) The growth of $k_{\max}$ is accelerated strongly with an increase in $\sigma_{\max}$ and slows down noticeably with an increase in recovery time between cycles $t^{\mathrm{c}}_{\mathrm{rec}}$.

The kinetics of recovery of PVA gel after multi-cycle deformation with a stress-controlled program (with maximum stress per cycle $\sigma_{\max} = 6$ kPa and various number of cycle N) is reported in Fig. 9, where elongation ratio k is plotted versus recovery time t_{rec} (t_{rec} denotes time measured from the instant when cyclic loading is terminated). Simulation is conducted for two recovery times between cycles ($t^{\mathrm{c}}_{\mathrm{rec}} = 1$ s and 1 min), and various N ranging from 1 to 1000. The following conclusions are drawn:

(I) At relatively small numbers of cycles ($N \leq 10$), the kinetics of recovery is exponential. At $N \geq 100$, two stages of recovery (rapid and slow) are clearly distinguished, and the decay in elongation ratio k with recovery time t_{rec} resembles that observed in Figs. 3 to 5. The time needed for total recovery of specimens increases from 5 min at $N = 1$ to several hours at $N > 100$.

(II) The elongation ratio at the beginning of recovery $k(0)$ grows monotonically with number of cycles N under fatigue conditions. Given N, this parameter decreases with recovery time between cycles $t^{\mathrm{c}}_{\mathrm{rec}}$. The effect of $t^{\mathrm{c}}_{\mathrm{rec}}$ is noticeable at relatively small N, but weakens with the growth of number of cycles. Surprisingly, the elongation ratio k after 10 min of recovery adopts higher values for multi-cycle deformation with $t^{\mathrm{c}}_{\mathrm{rec}} = 1$ min than for multi-cycle loading with $t^{\mathrm{c}}_{\mathrm{rec}} = 1$ s.

An important difference between the diagrams depicted in Fig. 9 and those presented in Figs. 3B, 4B and 5C consists in the mechanism of slowing down of self-recovery. Observations in the latter figures are attributed to deceleration of plastic flow, whereas results reported in Fig. 9 are obtained for the purely viscoelastic material.

To provide qualitative explanation of the recovery curves in Fig. 9, it is instructive to replace the entire ensemble of meso-domains in the transient network (characterized by the distribution function $f(u)$) with only two populations of meso-domains with short (small activation energy) and long (corresponding to the tail of the quasi-Gaussian function) times for rearrangement of temporary bonds.

When $N \leq 10$, the duration of multi-cycle deformation is insufficient for rearrangement of bonds with large activation energies. Only bonds with short times for detachment of chains from

temporary junctions are rearranged (adopt some $k > k(0)$ as elongation ratio for their reference state). Subsequent rearrangement of these junctions under recovery (when their reference state is determined by elongation ratio $k < k(0)$) reflects the one-step kinetics of self-recovery.

Under multi-cycle deformation with relatively large number of cycles $N \geq 100$, chains separate from temporary junctions with both short and long times of rearrangement. The higher N, the larger is the number of physical bonds with long times for rearrangement that adopt $k > k(0)$ as the elongation ratio for their reference state. When recovery starts, chains bridged by junctions with short rearrangement times return to their initial state rapidly (the initial stage of recovery). The second (slow) stage of recovery reflects detachment and re-attachment of chains linked by temporary bonds with long rearrangement times.

This scenario explains also why after 10 min of recovery the elongation ratio k for PVA gel subjected to fatigue test ($N = 1000$) with 1 min of rest between cycles exceeds that in the gel suffering 1 s of rest between cycles. The duration of the former test exceeds noticeably that for the latter experiment, which results in a higher number of bonds with long time for rearrangement that adopt $k > k(0)$ as the elongation ratio for their reference state and for which $t_{\rm rec} = 10$ min is insufficient to return into the initial state.

To examine how development of plastic deformation under cyclic loading affects the kinetics of self-recovery, simulation is conducted of the mechanical response of physically cross-linked AAm–AAc gel with the material constants listed in Tab. S4. Numerical analysis is performed for cyclic tests with constant strain rate $\dot{\epsilon} = 0.139$ s^{-1} and the strain-controlled program (fixed maximum elongation ratio per cycle $k_{\max} = 3.5$). To assess the effect of recovery time between cycles $t^{\rm c}_{\rm rec}$ on the mechanical response, we study multi-cycle deformation ($N = 50$) with $t^{\rm c}_{\rm rec} = 10$ and 60 min (these values are chosen to ensure that β_3 remains constant). The stress-strain diagrams are depicted in Fig. S10, and the decay in maximum stress per cycle $\sigma_{\max}$ with number of cycles n is demonstrated in Fig. 10. Results of simulation show that

(I) The shape of the stress-strain curves is strongly affected by recovery time between cycles (Fig. S10).

(II) The maximum stress per cycle is reduced with number of cycles n. The decay in $\sigma_{\max}(n)$ in Fig. 10 (induced by the viscoelastic and viscoplastic dissipation of energy) is substantially more pronounced than that in Fig. 7 (driven by the viscoelastic effects only).

(III) The rate of decrease in $\sigma_{\max}$ with number of cycles is reduced substantially with the growth of recovery time between cycles $t^{\rm c}_{\rm rec}$.

To evaluate the influence of number of cycles N under cyclic deformation on the rate of self-recovery, the governing equations are solved numerically for AAm-AAc gel subjected to multi-cycle deformation with $k_{\max} = 3.5$ and $t^{c}_{\rm rec} = 10$ min. Results of simulation are presented in Fig. 11. Fig. 11A illustrates the decrease in maximum stress per cycle with number of cycles, and Fig. 11B shows changes in elongation ratio k with recovery time $t_{\rm rec}$ after cyclic loadings with various N. Figs. 7, 9, and 11 imply that

(I) For the viscoelastic PVA gel subjected to cyclic deformation with a strain-controlled program, the decay in $\sigma_{\max}$ with n is linear at $n \geq 5$ (Fig. 7). Due to the viscoplastic effects, AAm-AAc gel reveals a strongly nonlinear decrease in $\sigma_{\max}(n)$ under the same deformation program (Fig. 11A).

(II) The growth of the number of cycles N results in a substantial increase in the duration of total self-recovery of AAm-AAc gel. Similarity of the diagrams depicted in Figs. 9B and 11B implies that this increase may be ascribed to the same physical mechanism (rearrangement of physical bonds with high activation energies under cyclic deformation with large N).

The following conclusions are drawn from the results of numerical analysis reported in Figs. 7 to 11:

(I) In agreement with available experimental data [35, 71, 72, 73], introduction of short intervals of self-recovery between subsequent cycles of deformation reduces damage accumulated in DN gels and leads to an increase in their lifetime. This result is obtained for cyclic deformations with strain-controlled (Fig. 7) and stress-controlled (Fig. 8) programs. It remains true for DN gels with purely viscoelastic behavior (PVA), and well as for hydrogels (AAm–AAc) that reveal the viscoelastoplastic response (Fig. 10). An advantage of our constitutive model is that it allows the lifetime under fatigue conditions to be predicted based on observations in tests with small number of cycles.

(II) The difference between one-stage [23, 31] and two-stage [32, 33, 34, 35] kinetics of self-recovery is explained in Section 3 by slowing down of the recovery process driven by evolution of micro-structure of a DN gel, Eq. (13). Simulation reveals another mechanism for transition from the exponential to non-exponential decay in residual strain when recovery is performed after multi-cycle deformation (Figs. 9 and 11). Based on the data reported in Fig. 9, this transition (which has not yet been observed in experiments) is associated with rearrangement of temporary bonds whose lifetimes exceed strongly the time needed to perform loading and unloading of a specimen.

5 Concluding remarks

A model is developed for the kinetics of self-recovery in a DN gel whose polymer network consists of two sub-networks with permanent (covalent) and temporary (non-covalent) bonds. The viscoelastic behavior reflects rearrangement of junctions in the transient network composed of meso-regions with various activation energies for detachment of chains. The viscoplastic response reflects sliding of junctions in the permanent network with respect to their reference positions. The rate of sliding (plastic flow) is governed by the energy of inter-chain interaction. Coefficients in the kinetic relation for plastic deformation adopt different values under the first loading, retraction, recovery, and reloading.

Self-recovery of a gel (a monotonic reduction in strain with time after the external load vanishes) reflects the balance between tensile stresses in chains of the permanent network (whose reference state coincides with the undeformed state of a sample) and compressive stresses in chains of the transient network that have rearranged (adopted the current state of the gel as their reference state) under cyclic deformation. The two-stage kinetics of recovery observed in experiments is explained by the fact that the rate of recovery is affected by (i) rearrangement of chains connected by temporary bonds and (ii) plastic flow of junctions in the permanent network.

The model is applied to fit experimental data in loading-unloading tests with various maximum elongation ratios, relaxation tests, and recovery tests (stretching-retraction-recovery-reloading-unloading) on a series of DN gels. Two advantages of the model are worth to be mentioning: (i) experimental stress–strain diagrams are described adequately by the governing equations, (ii) material parameters evolve consistently with experimental conditions.

Interactions between the self-recovery and fatigue phenomena in DN gels are studied numerically. Simulation shows that (i) the decay in maximum stress with number of cycles under the strain-controlled deformation program, and the growth of maximum strain under the stress-controlled program are strongly decelerated with an increase in recovery time between cycles, whereas (ii) the growth of the number of cycles under fatigue conditions results in a pronounced slowing down of the recovery process.

Acknowledgments

ADD and JDC acknowledge financial support by Innovationsfonden (Innovation Fund Denmark, project 5152-00002B). ND acknowledges fellowship support by Scientific and Technological Research

Council of Turkey (TUBITAK, project 1059B191601226).

References

[1] N. Annabi, A. Tamayol, J.A. Uquillas, M. Akbari, L.E. Bertassoni, C. Cha, G. Camci-Unal, M.R. Dokmeci, N.A. Peppas, A. Khademhosseini, *Adv. Mater.* **2014**, *26*, 85.

[2] N.A. Peppas, D.S. Van Blarcom, *J. Control. Release* **2016**, *240*, 142.

[3] T.E. Brown, K.S. Anseth, *Chem. Soc. Rev.* **2017**, *46*, 6532.

[4] F. Zhao, Y. Shi, L. Pan, G. Yu, *Acc. Chem. Res.* **2017**, *50*, 1734.

[5] S.Z. Bisri, S. Shimizu, M. Nakano, Y. Iwasa, *Adv. Mater.* **2017**, *29*, 1607054.

[6] C. Yang, Z. Suo, *Nat. Rev. Mater.* **2018**, *3*, 125.

[7] Y. Shi, L. Peng, G. Yu, *Nanoscale* **2015**, *7*, 12796.

[8] Y. Shi, J. Zhang, L. Pan, Y. Shi, G. Yu, *Nano Today* **2016**, *11*, 738.

[9] S. Lin, H. Yuk, T. Zhang, G.A. Parada, H. Koo, C. Yu, X. Zhao, *Adv. Mater.* **2016**, *28*, 4497.

[10] Y. Liu, K. He, G. Chen, W.R. Leow, X. Chen, *Chem. Rev.* **2017**, *117*, 12893.

[11] S. Park, K. Parida, P.S. Lee, *Adv. Energy Mater.* **2017**, *7*, 1701369.

[12] W. Xu, L.-B. Huang, M.-C. Wong, L. Chen, G. Bai, J. Hao, *Adv. Energy Mater.* **2017**, *7*, 1601529.

[13] T. Liu, M. Liu, S. Dou, J. Sun, Z. Cong, C. Jiang, C. Du, X. Pu, W. Hu, Z.L. Wang, *ACS Nano* **2018**, *12*, 2818.

[14] Y. Tanaka, R. Kuwabara, Y.-H. Na, T. Kurokawa, J.P. Gong, Y. Osada, *J. Phys. Chem. B* **2005**, *109*, 11559.

[15] J.P. Gong, *Science* **2014**, *344*, 161–162.

[16] E. Ducrot, Y. Chen, M. Bulters, R.P. Sijbesma, C. Creton, *Science* **2014**, *344*, 186.

[17] X. Zhao, *Soft Matter* **2014**, *10*, 672.

[18] C. Creton, *Macromolecules* **2017**, *50*, 8297.

[19] W. Wang, Y. Zhang, W. Liu, *Progr. Polym. Sci.* **2017**, *71*, 1.

[20] F. Meng, R.H. Pritchard, E.M. Terentjev, *Macromolecules* **2016**, *49*, 2843.

[21] A.D. Drozdov, R.K. Gupta, *Int. J. Eng. Sci.* **2003**, *41*, 2335.

[22] A.D. Drozdov, Q. Yuan, *Int. J. Solids Struct.* **2003**, *40*, 2321.

[23] R. Long, K. Mayumi, C. Creton, T. Narita, C.-Y. Hui, *Macromolecules* **2014**, *47*, 7243.

[24] V. Yesilyurt, A.M. Ayoob, E.A. Appel, J.T. Borenstein, R. Langer, D.G. Anderson, *Adv. Mater.* **2017**, *29*, 1605947.

[25] S.B. Myers, R.A. Register, *Macromolecules* **2009**, *42*, 6665.

[26] X. Liang, Y. Deng, X. Pei, K. Zhai, K. Xu, Y. Tan, X. Gong, P. Wang, *Soft Matter* **2017**, *13*, 2654.

[27] D. Wei, J. Yang, L. Zhu, F. Chen, Z. Tang, G. Qin, Q. Chen, *Polym. Testing* **2018**, *69*, 167.

[28] X. Yan, J. Yang, F. Chen, L. Zhu, Z. Tang, G. Qin, Q. Chen, G. Chen, *Compos. Sci. Technol.* **2018**, *163*, 81.

[29] J.-Y. Sun, X. Zhao, W.R.K. Illeperuma, O. Chaudhuri, K.H. Oh, D.J. Mooney, J.J. Vlassak, Z. Suo, *Nature* **2012**, *489*, 133.

[30] H. Fan, J. Wang, Z. Jin, *Macromolecules* **2018**, *51*, 1696.

[31] H. Ding, X.N. Zhang, S.Y. Zheng, Y. Song, Z.L. Wu, Q. Zheng, *Polymer* **2017**, *131*, 95.

[32] M.A. Haque, T. Kurokawa, G. Kamita, J.P. Gong, *Macromolecules* **2011**, *44*, 8916.

[33] T.L. Sun, T. Kurokawa, S. Kuroda, A.B. Ihsan, T. Akasaki, K. Sato, M.A. Haque, T. Nakajima, J.P. Gong, *Nat. Mater.* **2013**, *12*, 932.

[34] K. Peng, H. Yu, H. Yang, X. Hao, A. Yasin, X. Zhang, *Soft Matter* **2017**, *13*, 2135.

[35] B. Zhang, Z. Gao, G. Gao, W. Zhao, J. Li, X. Ren, *Macromol. Mater. Eng.* **2018**, *303*, 1800072.

[36] H. Chen, F. Yang, R. Hu, M. Zhang, B. Ren, X. Gong, J. Ma, B. Jiang, Q. Chen, J. Zheng, *J. Mater. Chem. B* **2016**, *4*, 5814.

[37] Y. Sun, G. Gao, G. Du, Y. Cheng, J. Fu, *ACS Macro Lett.* **2014**, *3*, 496.

[38] H.J. Zhang, T.L. Sun, A.K. Zhang, Y. Ikura, T. Nakajima, T. Nonoyama, T. Kurokawa, O. Ito, H. Ishitobi, J.P. Gong, *Adv. Mater.* **2016**, *28*, 4884.

[39] F. Chen, Q. Chen, L. Zhu, Z. Tang, Q. Li, G. Qin, J. Yang, Y. Zhang, B. Ren, J. Zheng, *Chem. Mater.* **2018**, *30*, 1743.

[40] R. Bai, Q. Yang, J. Tang, X.P. Morelle, J. Vlassak, Z. Suo, *Extreme Mech. Lett.* **2017**, *15*, 91.

[41] R. Bai, J. Yang, X.P. Morelle, C. Yang, Z. Suo, *ACS Macro Lett.* **2018**, *7*, 312.

[42] K.H. Vining, D.J. Mooney, *Nat. Rev. Mol. Cell Biol.* **2017**, *18*, 728.

[43] J. Guo, R. Long, K. Mayumi, C.-H. Hui, *Macromolecules* **2016**, *49*, 3497.

[44] X. Zhao, *J. Mech. Phys. Solids* **2012**, *60*, 319.

[45] F.J. Vernerey, R. Brighenti, R. Long, T. Shen, *Macromolecules* **2018**, *51*, 6609.

[46] R. Bai, J. Yang, Z. Suo, *Eur. J. Mech. A Solids* **2019**, *74*, 337.

[47] C. Xu, Q. Tang, H. Yang, K. Peng, X. Zhang, *Macromol. Chem. Phys.* **2018**, *219*, 1700636.

[48] S.Y. Zheng, H. Ding, J. Qian, J. Yin, Z.L. Wu, Y. Song, Q. Zheng, *Macromolecules* **2016**, *49*, 9637.

[49] P. Lin, S. Ma, X. Wang, F. Zhou, *Adv. Mater.* **2015**, *27*, 2054.

[50] M.S. Green, A.V. Tobolsky, *J. Chem. Phys.* **1946**, *14*, 80.

[51] F. Tanaka, S.F. Edwards, *Macromolecules* **1992**, *25*, 1516.

[52] G. Marckmann, E. Verron, L. Gornet, G. Chagnon, P. Charrier,, P. Fort, *J. Mech. Phys. Solids* **2002**, *50*, 2011.

[53] P. Sollich, *Phys. Rev. E* **1998**, *58*, 738.

[54] S.C. Grindy, M. Lenz, N. Holten-Andersen, *Macromolecules* **2016**, *49*, 8306.

[55] S. Tang, B.D. Olsen, *Macromolecules* **2016**, *49*, 9163.

[56] T.L. Sun, F. Luo, W. Hong, K. Cui, Y. Huang, H.J. Zhang, D.R. King, T. Kurokawa, T. Nakajima, J.P. Gong, *Macromolecules* **2017**, *50*, 2923.

[57] A.D. Drozdov, *Eng. Fract. Mech.* **2010**, *77*, 2277.

[58] L. Martinetti, J.M. Soulages, R.H. Ewoldt, *J. Rheol.* **2018**, *62*, 1271.

[59] A.D. Drozdov, J. deClaville Christiansen, *Macromolecules* **2018**, *51*, 1462.

[60] A.D. Drozdov, A.L. Kalamkarov, *Polym. Eng. Sci.* **1996**, *36*, 1907.

[61] S. Nam, K.H. Hu, M.J. Butte, O. Chaudhuri, *Proc. Nat. Acad. Sci. USA* **2016**, *113* 5492.

[62] F.J. Vernerey, R. Long, R. Brighenti, *J. Mech. Phys. Solids* **2017**, *107*, 1.

[63] F.J. Vernerey, *J. Mech. Phys. Solids* **2018**, *115*, 230.

[64] E. Filippidi, T.R. Cristiani, C.D. Eisenbach, J.H. Waite, J.N. Israelachvili, B.K. Ahn, M.T. Valentine, *Science* **2017**, *358*, 502.

[65] A.D. Drozdov, R.K. Gupta, *Int. J. Solids Struct.* **2003**, *40*, 6217.

[66] B. Wang, K.S. Fancey, *J. Appl. Polym. Sci.* **2017**, *134*, 44971.

[67] A.D. Drozdov, J. deClaville Christiansen, *Polymer* **2018**, *150*, 95.

[68] I. Iliopoulos,, R. Audebert, *Macromolecules* **1991**, *24*, 2566.

[69] H. Kaczmarek, A. Szalla, A. Kaminska, *Polymer* **2001**, *42*, 6057.

[70] Y.-L. Rao, A. Chortos, R. Pfattner, F. Lissel, Y.-C. Chiu, V. Feig, J. Xu, T. Kurosawa, X. Gu, C. Wang, M. He, J.W. Chung, Z. Bao, *J. Am. Chem. Soc.* **2016**, *138*, 6020.

[71] Y. Yang, X. Wang, F. Yang, H. Shen,, D. Wu, *Adv. Mater.* **2016**, *28*, 7178.

[72] Y. Yang, X. Wang, F. Yang, L. Wang, D. Wu, *Adv. Mater.* **2018**, *30*, 1707071.

[73] X.-H. Wang, F. Song, D. Qian, Y.-D. He, W.-C. Nie, X.-L. Wang, Y.-Z. Wang, *Chem. Eng. J.* **2018**, *349*, 588.

List of figures

Figure 1: A: Tensile stress σ versus elongation ratio k. Circles: experimental data [23] on PVA gel in cyclic test with strain rate $\dot{\epsilon} = 0.03$ s^{-1} and maximum elongation ratio $k_{\max} = 2$. Solid line: results of simulation. B: Tensile stress σ versus relaxation time $t_{\rm rel}$. Circles: experimental data [23] in relaxation test with strain rate under stretching $\dot{\epsilon} = 0.2$ s^{-1} and elongation ratio $k = 1.1$. Solid line: results of simulation. C: Tensile stress σ versus elongation ratio k. Unfilled circles: experimental data [23] in cyclic test with strain rate $\dot{\epsilon} = 0.03$ s^{-1} and $k_{\max} = 2$. Other symbols: predictions of the model for the second cycle of deformation after recovery for various times $t_{\rm rec}$. D: Elongation ratio k versus recovery time $t_{\rm rec}$. Solid line: results of simulation for the recovery test followed cyclic deformation with strain rate $\dot{\epsilon} = 0.03$ s^{-1} and $k_{\max} = 2$.

Figure 2: A: Tensile stress σ versus elongation ratio k. Symbols: experimental data [47] on MAAc-VP-PEGMA gel in cyclic tests with strain rate $\dot{\epsilon} = 0.154$ s^{-1} and various maximum elongation ratios $k_{\max}$. Solid lines: results of simulation. B: Tensile stress σ versus elongation ratio k. Symbols: experimental data [47] in cyclic tests with $k_{\max} = 6$. Solid line: results of simulation. C: Tensile stress σ versus elongation ratio k. Symbols: experimental data [47] in recovery tests with $k_{\max} = 3$. Circles: loading–unloading diagram for the first cycle of deformation. Other symbols: loading paths for the second cycle after recovery for various times $t_{\rm rec}$ min. Solid lines: results of simulation. D: Tensile stress σ versus elongation ratio k. Solid line: results of simulation for cyclic deformation with $k_{\max} = 6$. Circles: prediction of the model for the second cycle of deformation after 30 min of recovery. E: Elongation ratio k versus recovery time $t_{\rm rec}$. Circles: experimental data [47] in recovery tests followed cyclic deformation with $k_{\max} = 3$. Solid line: results of simulation. F: Elongation ratio k versus recovery time $t_{\rm rec}$. Solid line: results of simulation for recovery test followed cyclic deformation with $k_{\max} = 6$.

Figure 3: A: Tensile stress σ versus elongation ratio k. Circles: experimental data [48] on physically cross-linked AAm-AAc gels in cyclic test with strain rate $\dot{\epsilon} = 0.139$ s^{-1} and maximum elongation ratio $k_{\max} = 3.5$. Other symbols: experimental data [48] along the reloading paths after recovery for various times $t_{\rm rec}$ min. Solid lines: results of simulation. B: Elongation ratio k versus recovery time $t_{\rm rec}$. Circles: experimental data [48] in recovery tests followed cyclic deformation with $k_{\max} = 3.5$. Solid line: results of simulation.

Figure 4: A: Tensile stress σ versus elongation ratio k. Circles: experimental data [34] on AAm-AAc-ODA gel in cyclic test with strain rate $\dot{\epsilon} = 0.083$ s^{-1} and maximum elongation ratio $k_{\max} = 2.5$. Other symbols: experimental data [34] along the reloading paths after recovery for various times $t_{\rm rec}$ min. Solid lines: results of simulation. B: Elongation ratio k versus recovery time $t_{\rm rec}$. Circles: experimental data [34] in recovery tests followed cyclic deformation with $k_{\max} = 2.5$. Solid line: results of simulation.

Figure 5: A: Tensile stress σ versus elongation ratio k. Symbols: experimental data [49] on double cross-linked AAm–AAc gel in cyclic tests with strain rate $\dot{\epsilon} = 0.083$ s^{-1} and various maximum elongation ratios $k_{\max}$. Solid lines: results of simulation. B: Tensile stress σ versus elongation ratio k. Circles: experimental data [49] in loading–unloading test with strain rate $\dot{\epsilon} = 0.083$ s^{-1} and maximum elongation ratio $k_{\max} = 4$. Other symbols: experimental data [49] along the reloading paths on samples recovered for various times $t_{\rm rec}$ min. Solid lines: results of simulation. C: Elongation ratio k versus recovery time $t_{\rm rec}$. Circles: experimental data [49] in recovery test followed cyclic deformation with $k_{\max} = 4$. Solid line: results of simulation.

Figure 6: A: Tensile stress σ versus elongation ratio k. Circles: experimental data [70] on PDMS-$FeCl_2$ elastomer in cyclic test with strain rate $\dot{\epsilon} = 0.0167$ s^{-1} and maximum elongation ratio $k_{\max} = 2$. Solid line: results of simulation. B: Ratio of tensile stresses $S = \sigma(t_{\rm rel})/\sigma(0)$ versus relaxation time $t_{\rm rel}$. Circles: experimental data [70] in relaxation test with strain rate under stretching $\dot{\epsilon} = 0.0167$ s^{-1} and elongation ratio $k_{\max} = 1.03$. Solid line: results of simulation.

Figure 7: Maximum stress per cycle $\sigma_{\max}$ versus number of cycles n. Symbols: predictions of the model for multi-cycle tests on PVA gel with strain rate $\dot{\epsilon} = 0.03$ s^{-1}, maximum elongation ratio per cycle $k_{\max} = 2$, and various recovery times between cycles $t^{\rm c}_{\rm rec}$.

Figure 8: A: Maximum elongation ratio per cycle $k_{\max}$ versus number of cycles n. Symbols: predictions of the model for multi-cycle tests with maximum stress per cycle $\sigma_{\max} = 5$ kPa, and various recovery times between cycles $t^{\rm c}_{\rm rec}$. B: Maximum elongation ratio per cycle $k_{\max}$ versus number of cycles n. Symbols: predictions of the model for multi-cycle tests with recovery time between cycles $t^{\rm c}_{\rm rec} = 1$ s, and various maximum stresses per cycle $\sigma_{\max}$ kPa.

Figure 9: Elongation ratio k versus recovery time $t_{\rm rec}$. Symbols: results of simulation for multi-cycle tests on PVA gel with strain rate $\dot{\epsilon} = 0.03$ s^{-1}, maximum stress per cycle $\sigma_{\max} = 6$ kPa,

recovery time between cycles $t^{\mathrm{c}}_{\mathrm{rec}}$, and various number of cycles N. A: $t^{\mathrm{c}}_{\mathrm{rec}} = 1$ s. B: $t^{\mathrm{c}}_{\mathrm{rec}} = 1$ min.

Figure 10: Maximum stress per cycle $\sigma_{\max}$ versus number of cycles n. Solid lines and symbols: predictions of the model for multi-cycle tests on AAm-AAc gel with strain rate $\dot{\epsilon} = 0.139\ \mathrm{s}^{-1}$, maximum elongation ratio $k_{\max} = 3.5$, and various recovery times between cycles $t^{\mathrm{c}}_{\mathrm{rec}}$.

Figure 11: A: Maximum stress per cycle $\sigma_{\max}$ versus number of cycles n. B: Elongation ratio k versus recovery time t_{rec}. Symbols: predictions of the model for multi-cycle tests on AAm-AAc gel with strain rate $\dot{\epsilon} = 0.139\ \mathrm{s}^{-1}$, maximum elongation ratio per cycle $k_{\max} = 3.5$, recovery time between cycles $t^{\mathrm{c}}_{\mathrm{rec}} = 10$ min, and various numbers of cycles N.

Supporting Information
Self-recovery and fatigue of double-network hydrogels with permanent and reversible bonds

A.D. Drozdov[1], N. Dusunceli[2], C.-G. Sanporean[1], J. deClaville Christiansen[1]
[1]Department of Materials and Production
Aalborg University, Fibigerstraede 16, Aalborg 9220, Denmark
[2]Department of Mechanical Engineering
Aksaray University, Aksaray 68100, Turkey

Constitutive model

A double-network (DN) gel is modeled as a two-phase continuum composed of an equivalent polymer network and water. The solid and fluid phases are treated as immiscible interpenetrating media. The polymer network is thought of as a superposition of two networks: permanent (chains are bridged by covalent permanent cross-links) and transient (chains are connected by non-covalent reversible junctions).

1 Kinematic relations

The initial configuration of a gel coincides with that of an undeformed dry specimen. Transformation of the initial configuration into the actual configuration at time t is described by the deformation gradient $\mathbf{F}(t)$. According to the affinity hypothesis, the deformation gradients for the permanent and transient networks coincide with that for macro-deformation.

The molecular incompressibility condition reads

$$J = 1 + Q, \tag{S-1}$$

where $J = \det \mathbf{F}$, $Q = Cv$ stands for degree of swelling, C is concentration of water molecules (number of molecules per unit volume in the initial state), and v is the characteristic volume of a molecule. Eq. (S-1) means that volume deformation of a gel is induced by changes in water content only.

1.1 Permanent network

The reference (stress-free) state of the permanent network before application of external loads coincides with the as-prepared state of a gel. Transformation of the initial state into the reference state is described by the deformation gradient $\mathbf{F}_\mathrm{r}$ (the subscript "r" stands for reference). For an isotropic polymer network, we set

$$\mathbf{F}_\mathrm{r} = (1 + Q_\mathrm{r})^{\frac{1}{3}}\mathbf{I}, \tag{S-2}$$

where $\mathbf{I}$ is the unit tensor, $Q_\mathrm{r} = C_\mathrm{r}v$, and C_r stands for concentration of water molecules in the as-prepared gel.

Denote by $\mathbf{F}_\mathrm{p}(t)$ the deformation gradient for plastic deformation of the permanent network (transition from the initial state into the stress-free state at an arbitrary instant $t \geq 0$). Bearing in mind that $\mathbf{F}_\mathrm{p}(0) = \mathbf{F}_\mathrm{r}$, we find from Eq. (S-2) that

$$\mathbf{F}_\mathrm{p}(0) = (1 + Q_\mathrm{r})^{\frac{1}{3}}\mathbf{I}. \tag{S-3}$$

The multiplicative decomposition formula implies that

$$\mathbf{F} = \mathbf{F}_\mathrm{e} \cdot \mathbf{F}_\mathrm{p}, \tag{S-4}$$

where $\mathbf{F}_\mathrm{e}$ is the deformation gradient for elastic deformation, and the dot stands for inner product. The velocity gradient for macro-deformation is given by

$$\mathbf{L} = \dot{\mathbf{F}} \cdot \mathbf{F}^{-1}, \tag{S-5}$$

where the superscript dot stands for the derivative with respect to time. Combination of Eqs. (S-4) and (S-5) implies that

$$\mathbf{L} = \mathbf{L}_\mathrm{e} + \mathbf{L}_\mathrm{p}, \tag{S-6}$$

where

$$\mathbf{L}_\mathrm{e} = \dot{\mathbf{F}}_\mathrm{e} \cdot \mathbf{F}_\mathrm{e}^{-1}, \qquad \mathbf{L}_\mathrm{p} = \mathbf{F}_\mathrm{e} \cdot \mathbf{l}_\mathrm{p} \cdot \mathbf{F}_\mathrm{e}^{-1}, \qquad \mathbf{l}_\mathrm{p} = \dot{\mathbf{F}}_\mathrm{p} \cdot \mathbf{F}_\mathrm{p}^{-1}. \tag{S-7}$$

Following the conventional approach, we disregard plastic spin and presume the velocity gradient $\mathbf{l}_\mathrm{p}$ to be symmetric,

$$\mathbf{l}_\mathrm{p} = \mathbf{d}_\mathrm{p}, \tag{S-8}$$

where

$$\mathbf{d}_\mathrm{p} = \frac{1}{2}(\mathbf{l}_\mathrm{p} + \mathbf{l}_\mathrm{p}^\top) \tag{S-9}$$

is the rate-of-strain tensor for plastic deformation, and $\top$ stands for transpose. It follows from Eqs. (S-7) and (S-8) that the tensor $\mathbf{F}_\mathrm{p}$ obeys the differential equation

$$\dot{\mathbf{F}}_\mathrm{p} = \mathbf{d}_\mathrm{p} \cdot \mathbf{F}_\mathrm{p} \tag{S-10}$$

with initial condition (S-3).

Combination of Eqs. (S-6) and (S-7) results in

$$\mathbf{D} = \mathbf{D}_\mathrm{e} + \mathbf{D}_\mathrm{p}, \tag{S-11}$$

where

$$\mathbf{D} = \frac{1}{2}(\mathbf{L} + \mathbf{L}^\top), \qquad \mathbf{D}_\mathrm{e} = \frac{1}{2}(\mathbf{L}_\mathrm{e} + \mathbf{L}_\mathrm{e}^\top), \qquad \mathbf{D}_\mathrm{p} = \frac{1}{2}(\mathbf{L}_\mathrm{p} + \mathbf{L}_\mathrm{p}^\top) \tag{S-12}$$

are the rate-of-strain tensors for macro-deformation, elastic deformation, and plastic deformation, respectively, and

$$\mathbf{D}_\mathrm{p} = \frac{1}{2}\Big(\mathbf{F}_\mathrm{e} \cdot \mathbf{d}_\mathrm{p} \cdot \mathbf{F}_\mathrm{e}^{-1} + \mathbf{F}_\mathrm{e}^{-\top} \cdot \mathbf{d}_\mathrm{p} \cdot \mathbf{F}_\mathrm{e}^{\top}\Big). \tag{S-13}$$

The left Cauchy–Green tensors for elastic and plastic deformation read

$$\mathbf{B}_\mathrm{e} = \mathbf{F}_\mathrm{e} \cdot \mathbf{F}_\mathrm{e}^\top, \qquad \mathbf{b}_\mathrm{p} = \mathbf{F}_\mathrm{p} \cdot \mathbf{F}_\mathrm{p}^\top. \tag{S-14}$$

Differentiating Eqs. (S-14) with respect to time and using Eqs. (S-7) and (S-10), we find that

$$\dot{\mathbf{B}}_\mathrm{e} = \mathbf{L}_\mathrm{e} \cdot \mathbf{B}_\mathrm{e} + \mathbf{B}_\mathrm{e} \cdot \mathbf{L}_\mathrm{e}^\top, \qquad \dot{\mathbf{b}}_\mathrm{p} = \mathbf{d}_\mathrm{p} \cdot \mathbf{b}_\mathrm{p} + \mathbf{b}_\mathrm{p} \cdot \mathbf{d}_\mathrm{p}. \tag{S-15}$$

Denote by $I_{\mathrm{e}1}$, $I_{\mathrm{e}2}$, $I_{\mathrm{e}3}$ the principal invariants of the Cauchy–Green tensor for elastic deformation, and by $I_{\mathrm{p}1}$, $I_{\mathrm{p}2}$, $I_{\mathrm{p}3}$ the principal invariants of the Cauchy–Green tensor for plastic deformation. It follows from Eq. (S-15) that the derivatives of these functions with respect to time obey the differential equations

$$\dot{I}_{\mathrm{e}1} = 2\mathbf{B}_\mathrm{e} : \mathbf{D}_\mathrm{e}, \qquad \dot{I}_{\mathrm{e}2} = 2\Big(I_{\mathrm{e}2}\mathbf{I} - I_{\mathrm{e}3}\mathbf{B}_\mathrm{e}^{-1}\Big) : \mathbf{D}_\mathrm{e}, \qquad \dot{I}_{\mathrm{e}3} = 2I_{\mathrm{e}3}\mathbf{I} : \mathbf{D}_\mathrm{e}, \tag{S-16}$$

$$\dot{I}_{\mathrm{p}1} = 2\mathbf{b}_\mathrm{p} : \mathbf{d}_\mathrm{p}, \qquad \dot{I}_{\mathrm{p}2} = 2\Big(I_{\mathrm{p}2}\mathbf{I} - I_{\mathrm{p}3}\mathbf{b}_\mathrm{p}^{-1}\Big) : \mathbf{d}_\mathrm{p}, \qquad \dot{I}_{\mathrm{p}3} = 2I_{\mathrm{p}3}\mathbf{I} : \mathbf{d}_\mathrm{p}, \tag{S-17}$$

where the colon stands for convolution. Replacing $\mathbf{D}_\mathrm{e}$ in Eq. (S-16) by means of Eq. (S-11) and using Eq. (S-13), we find that

$$\begin{aligned}
\dot{I}_{\mathrm{e}1} &= 2\Big(\mathbf{B}_\mathrm{e} : \mathbf{D} - \mathbf{C}_\mathrm{e} : \mathbf{d}_\mathrm{p}\Big), \\
\dot{I}_{\mathrm{e}2} &= 2\Big[\Big(I_{\mathrm{e}2}\mathbf{I} - I_{\mathrm{e}3}\mathbf{B}_\mathrm{e}^{-1}\Big) : \mathbf{D} - \Big(I_{\mathrm{e}2}\mathbf{I} - I_{\mathrm{e}3}\mathbf{C}_\mathrm{e}^{-1}\Big) : \mathbf{d}_\mathrm{p}\Big], \\
\dot{I}_{\mathrm{e}3} &= 2I_{\mathrm{e}3}\Big(\mathbf{I} : \mathbf{D} - \mathbf{I} : \mathbf{d}_\mathrm{p}\Big),
\end{aligned} \tag{S-18}$$

where

$$\mathbf{C}_\mathrm{e} = \mathbf{F}_\mathrm{e}^\top \cdot \mathbf{F}_\mathrm{e} \tag{S-19}$$

stands for the right Cauchy–Green tensor for elastic deformation.

Eqs. (S-17) and (S-18) are valid for arbitrary elastic and plastic deformations. We presume plastic deformation to be volume-preserving (isochoric), which means that

$$I_{\rm p3} = 1. \tag{S-20}$$

Combination of Eqs. (S-17) and (S-20) results in

$$\mathbf{I} : \mathbf{d}_{\rm p} = 0, \tag{S-21}$$

which means that the tensor $\mathbf{d}_{\rm p}$ is traceless. It follows from Eqs. (S-17) and (S-21) that the functions $I_{\rm p1}$, $I_{\rm p2}$ are governed by the equations

$$\dot{I}_{\rm p1} = 2\mathbf{b}_{\rm p} : \mathbf{d}_{\rm p}, \qquad \dot{I}_{\rm p2} = -2\mathbf{b}_{\rm p}^{-1} : \mathbf{d}_{\rm p}. \tag{S-22}$$

Eqs. (S-18) and (S-21) imply that the functions $I_{\rm e1}$, $I_{\rm e2}$, $I_{\rm e3}$ obey the equations

$$\begin{aligned} \dot{I}_{\rm e1} &= 2\Big(\mathbf{B}_{\rm e} : \mathbf{D} - \mathbf{C}_{\rm e} : \mathbf{d}_{\rm p}\Big), \\ \dot{I}_{\rm e2} &= 2\Big[\Big(I_{\rm e2}\mathbf{I} - I_{\rm e3}\mathbf{B}_{\rm e}^{-1}\Big) : \mathbf{D} + I_{\rm e3}\mathbf{C}_{\rm e}^{-1} : \mathbf{d}_{\rm p}\Big], \\ \dot{I}_{\rm e3} &= 2I_{\rm e3}(\mathbf{I} : \mathbf{D}). \end{aligned} \tag{S-23}$$

Differentiating Eq. (S-19) with respect to time and using Eqs. (S-7) and (S-12), and find that

$$\dot{\mathbf{C}}_{\rm e} = 2\mathbf{F}_{\rm e}^{\top} \cdot \mathbf{D}_{\rm e} \cdot \mathbf{F}_{\rm e}. \tag{S-24}$$

Combination of Eq. (S-24) with Eqs. (S-11) and (S-13) yields

$$\dot{\mathbf{C}}_{\rm e} = 2\mathbf{F}_{\rm e}^{\top} \cdot \mathbf{D} \cdot \mathbf{F}_{\rm e} - (\mathbf{C}_{\rm e} \cdot \mathbf{d}_{\rm p} + \mathbf{d}_{\rm p} \cdot \mathbf{C}_{\rm e}). \tag{S-25}$$

1.2 Transient network

To describe the response of the transient network, we denote by τ an instant when a polymer chain merges with the network, and distinguish chains connected to the network before loading ($\tau = 0$) and those attached to the network under deformation ($\tau > 0$).

For a chain with $\tau = 0$, transformation from the initial state into the reference state is determined by the deformation gradient $\mathbf{F}_{\rm r}$, and deformation gradient for elastic deformation $\mathbf{f}_0(t)$ is given by

$$\mathbf{f}_0(t) = \mathbf{F}(t) \cdot \mathbf{F}_{\rm r}^{-1}. \tag{S-26}$$

For a chain with $\tau > 0$, the reference state is presumed to coincide with the actual state of the network at instant τ. This means that stresses in a dangling chain have relaxed entirely before this chain joins the network, and the deformation gradient for elastic deformation reads

$$\mathbf{f}_\tau(t) = \mathbf{F}(t) \cdot \mathbf{F}^{-1}(\tau). \tag{S-27}$$

The corresponding left Cauchy–Green tensors are determined by

$$\mathbf{b}_0 = \mathbf{f}_0 \cdot \mathbf{f}_0^\top, \qquad \mathbf{b}_\tau = \mathbf{f}_\tau \cdot \mathbf{f}_\tau^\top. \tag{S-28}$$

Differentiating Eqs. (S-28) with respect to time t and using Eqs. (S-5), (S-26) and (S-27), we find that

$$\dot{\mathbf{b}}_0 = \mathbf{L} \cdot \mathbf{b}_0 + \mathbf{b}_0 \cdot \mathbf{L}^\top, \qquad \dot{\mathbf{b}}_\tau = \mathbf{L} \cdot \mathbf{b}_\tau + \mathbf{b}_\tau \cdot \mathbf{L}^\top. \tag{S-29}$$

Denote by I_{01}, I_{02}, I_{03} and $I_{\tau 1}$, $I_{\tau 2}$, $I_{\tau 3}$ the principal invariants of the tensors $\mathbf{b}_0$ and $\mathbf{b}_\tau$, respectively. It can be shown by analogy with Eq. (S-16) that these functions are governed by the differential equations

$$\begin{aligned} &\dot{I}_{01} = 2\mathbf{b}_0 : \mathbf{D}, \qquad \dot{I}_{02} = 2\Big(I_{02}\mathbf{I} - I_{03}\mathbf{b}_0^{-1}\Big) : \mathbf{D}, \qquad \dot{I}_{03} = 2I_{03}\mathbf{I} : \mathbf{D}, \\ &\dot{I}_{\tau 1} = 2\mathbf{b}_\tau : \mathbf{D}, \qquad \dot{I}_{\tau 2} = 2\Big(I_{\tau 2}\mathbf{I} - I_{\tau 3}\mathbf{b}_\tau^{-1}\Big) : \mathbf{D}, \qquad \dot{I}_{\tau 3} = 2I_{\tau 3}\mathbf{I} : \mathbf{D}. \end{aligned} \tag{S-30}$$

To describe rearrangement of the transient network (separation of active chains from temporary junctions and attachment of dangling chains to the network), we presume the network to be inhomogeneous and composed of meso-domains with various activation energies U for detachment of chains from temporary junctions. The rate of detachment Γ in a meso-domain with activation energy U is governed by the Eyring equation

$$\Gamma = \bar{\gamma} \exp\Big(-\frac{U}{k_{\mathrm{B}}T}\Big),$$

where $\bar{\gamma}$ is an attempt rate, k_{B} denotes Boltzmann's constant, and T stands for the absolute temperature. Introducing the dimensionless activation energy

$$u = \frac{U}{k_{\mathrm{B}}T},$$

we present this relation in the form

$$\Gamma(t, u) = \bar{\gamma}(t) \exp(-u), \tag{S-31}$$

where the dependence of $\bar{\gamma}$ on time reflects the effect of mechanical factors on the rearrangement process.

Denote by N_{a} the number of active chains in the transient network (per unit volume in the initial state). This quantity is presumed to be independent of time. The number of active chains in meso-domains with dimensionless activation energy u reads

$$\bar{N}_{\mathrm{a}}(u) = N_{\mathrm{a}} f(u), \tag{S-32}$$

where $f(u)$ is the distribution function for meso-domains with various activation energies. This function obeys the normalization condition

$$\int_0^\infty f(u)\mathrm{d}u = 1. \tag{S-33}$$

The current state of the transient network is uniquely determined by the function of three variables $n(t,\tau,u)$ that equals the number (per unit volume in the initial state) of active chains at time $t \geq 0$ that have returned into the active state before instant $\tau \leq t$ and belong to a meso-domain with activation energy u.

In particular, $n(t,0,u)$ denotes concentration of chains in meso-domains with activation energy u that have been attached to the network before loading and remain active at time t, and $n(t,t,u)$ stands for concentration of active chains at time $t \geq 0$ in meso-domains with activation energy u. Bearing in mind that $\bar{N}_\mathrm{a}$ is independent of time, we conclude from Eq. (S-32) that

$$n(t,t,u) = n(0,0,u) = N_\mathrm{a} f(u). \tag{S-34}$$

The number of chains that were active at the initial instant and separate from their junctions within the interval $[t, t+\mathrm{d}t]$ reads

$$-\frac{\partial n}{\partial t}(t,0,u)\ \mathrm{d}t,$$

the number of dangling chains that return into the active state within the interval $[\tau, \tau+\mathrm{d}\tau]$ is given by $\varphi(\tau,u)\mathrm{d}\tau$ with

$$\varphi(\tau,u) = \frac{\partial n}{\partial \tau}(t,\tau,u)\Big|_{t=\tau}, \tag{S-35}$$

and the number of chains that merged (for the last time) with the network within the interval $[\tau, \tau+\mathrm{d}\tau]$ and detach from their junctions within the interval $[t, t+\mathrm{d}t]$ is determined as

$$-\frac{\partial^2 n}{\partial t \partial \tau}(t,\tau,u)\ \mathrm{d}t\mathrm{d}\tau.$$

Detachment of active chains from their junctions is described by the first-order kinetic equations

$$\frac{\partial n}{\partial t}(t,0,u) = -\Gamma(t,u) n(t,0,u), \qquad \frac{\partial^2 n}{\partial t \partial \tau}(t,\tau,u) = -\Gamma(t,u)\frac{\partial n}{\partial \tau}(t,\tau,u), \tag{S-36}$$

which mean that the number of active chains detaching from their junctions per unit time is proportional to the number of active chains in an appropriate meso-region. Integrating Eq. (S-36) with initial conditions (S-34) and (S-35) we find that

$$n(t,0,u) = N_\mathrm{a} f(u) \exp\Big[-\int_0^t \Gamma(s,u)\mathrm{d}s\Big], \qquad \frac{\partial n}{\partial \tau}(t,\tau,u) = \varphi(\tau,u)\exp\Big[-\int_\tau^t \Gamma(s,u)\mathrm{d}s\Big]. \tag{S-37}$$

Inserting expressions (S-37) into the equality

$$n(t,t,u) = n(t,0,u) + \int_0^t \frac{\partial n}{\partial \tau}(t,\tau,u)\mathrm{d}\tau,$$

and using Eq. (S-34), we arrive at the formula

$$\varphi(t,u) = \Gamma(t,u) N_{\mathrm{a}} f(u). \tag{S-38}$$

2 Strain energy density

Denote by W the strain energy density (per unit volume) of the equivalent polymer network. For the network consisting of two parts (permanent and transient), the function W reads

$$W = W_1 + W_2, \tag{S-39}$$

where W_1, W_2 are the specific mechanical energies of chains belonging to the permanent and transient networks.

The strain energy density of the permanent network is given by

$$W_1 = W_{\mathrm{e}} + W_{\mathrm{p}}, \tag{S-40}$$

where the mechanical energy stored in chains W_{e} depends on the principal invariants $I_{\mathrm{e}1}$, $I_{\mathrm{e}2}$, $I_{\mathrm{e}3}$ of the Cauchy–Green tensor for elastic deformation $\mathbf{B}_{\mathrm{e}}$, and the energy of inter-chain interaction W_{p} is treated as a function of the principal invariants $I_{\mathrm{p}1}$, $I_{\mathrm{p}2}$ of the Cauchy–Green tensor $\mathbf{b}_{\mathrm{p}}$.

To calculate the strain energy density of the transient network W_2, we introduce the mechanical energy per chain w and suppose that it depends on the principal invariants $I_{\tau 1}$, $I_{\tau 2}$, $I_{\tau 3}$ of the Cauchy–Green tensor $\mathbf{b}_\tau$ ($\tau \geq 0$). At an arbitrary instant $t \geq 0$, the quantity W_2 is determined by

$$\begin{aligned} W_2(t) \;=\; & \int_0^\infty \Bigg[n(t,0,u) w\Big(I_{01}(t), I_{02}(t), I_{03}(t)\Big) \\ & + \int_0^t \frac{\partial n}{\partial \tau}(t,\tau,u) w\Big(I_{\tau 1}(t), I_{\tau 2}(t), I_{\tau 3}(t)\Big) \mathrm{d}\tau \Bigg] \mathrm{d}u, \end{aligned} \tag{S-41}$$

where the first term stands for the strain energy (per unit volume) of chains that have merged with the network before deformation and remain active at time t, and the other term expresses the energy stored in chains that have attached the network at various instants $\tau \leq t$ and have not separated from the network within the intervals $[\tau, t]$.

3 Constitutive equations

We consider a DN gel with degree of swelling Q_{r} in the as-prepared state that has been swollen until equilibrium before deformation. Degree of swelling in the equilibrium state equals Q. After equilibration, external forces are applied to the sample. The rate of loading is presumed to exceed strongly the rate of diffusion of solvent, which implies that transport of water molecules under

deformation is disregarded, and degree of swelling Q remains constant. This assumption together with molecular incompressibility condition (S-1) implies that J is time-independent. The latter means that under deformation,

$$\mathbf{I} : \mathbf{D} = 0, \tag{S-42}$$

where the rate-of-strain tensor $\mathbf{D}$ is given by Eq. (S-12).

Constitutive equations for a gel under isothermal deformation are developed by means of the free energy imbalance inequality

$$\dot{W} - \Phi_{\mathrm{mec}} \le 0, \tag{S-43}$$

where

$$\Phi_{\mathrm{mec}} = J\boldsymbol{\Sigma} : \mathbf{D} \tag{S-44}$$

denotes the work (per unit volume in the initial state and unit time) produced by external loads, and $\boldsymbol{\Sigma}$ stands for the Cauchy stress tensor.

Eq. (S-43) is fulfilled when the deformation gradient $\mathbf{F}$ obeys Eq. (S-42). To account for this condition, we multiply Eq. (S-42) by $J\Pi$, where Π is an arbitrary function (pressure treated as a Lagrange multiplier) and add the result to Eq. (S-43). Using Eqs. (S-22), (S-23), (S-30), (S-36), (S-39)–(S-41) and (S-44), we arrive at the inequality

$$[2\mathbf{K}_{\mathrm{e}} - J(\boldsymbol{\Sigma} + \Pi\mathbf{I})] : \mathbf{D} + 2\mathbf{K}_{\mathrm{p}} : \mathbf{d}_{\mathrm{p}} - \Xi \le 0 \tag{S-45}$$

with

$$\begin{aligned}
\mathbf{K}_{\mathrm{e}} &= \Big[W_{\mathrm{e},1}\mathbf{B}_{\mathrm{e}} - W_{\mathrm{e},2}I_{\mathrm{e}3}\mathbf{B}_{\mathrm{e}}^{-1} + \Big(W_{\mathrm{e},2}I_{\mathrm{e}2} + W_{\mathrm{e},3}I_{\mathrm{e}3}\Big)\mathbf{I}\Big] \\
&\quad + \int_0^\infty \Big\{ n(t,0,u)\Big[w_{,1}\mathbf{b}_0 - w_{,2}I_{03}\mathbf{b}_0^{-1} + \Big(w_{,2}I_{02} + w_{,3}I_{03}\Big)\mathbf{I}\Big] \\
&\quad + \int_0^t \frac{\partial n}{\partial \tau}(t,\tau,u)\Big[w_{,1}\mathbf{b}_\tau - w_{,2}I_{\tau 3}\mathbf{b}_\tau^{-1} + \Big(w_{,2}I_{\tau 2} + w_{,3}I_{\tau 3}\Big)\mathbf{I}\Big]\mathrm{d}\tau\Big\}\mathrm{d}u, \\
\mathbf{K}_{\mathrm{p}} &= \Big[\Big(W_{\mathrm{p},1}\mathbf{b}_{\mathrm{p}} - W_{\mathrm{p},2}I_{\mathrm{p}3}\mathbf{b}_{\mathrm{p}}^{-1}\Big) - \Big(W_{\mathrm{e},1}\mathbf{C}_{\mathrm{e}} - W_{\mathrm{e},2}I_{\mathrm{e}3}\mathbf{C}_{\mathrm{e}}^{-1}\Big)\Big]', \\
\Xi &= \int_0^\infty \Gamma(t,u)\Big[n(t,0,u)w\Big(I_{01}(t), I_{02}(t), I_{03}(t)\Big) \\
&\quad + \int_0^t \frac{\partial n}{\partial \tau}(t,\tau,u)w\Big(I_{\tau 1}(t), I_{\tau 2}(t), I_{\tau 3}(t)\Big)\mathrm{d}\tau\Big]\mathrm{d}u,
\end{aligned}$$

where

$$W_{\mathrm{e},m} = \frac{\partial W_{\mathrm{e}}}{\partial I_{\mathrm{e}m}}, \qquad W_{\mathrm{p},m} = \frac{\partial W_{\mathrm{p}}}{\partial I_{\mathrm{p}m}}, \qquad w_{,m} = \frac{\partial w}{\partial I_{\tau m}},$$

and the prime stands for the deviatoric component of a tensor ($\mathbf{A}' = \mathbf{A} - \frac{1}{3}\mathbf{A} : \mathbf{I}$ for any $\mathbf{A}$).

Keeping in mind that $\mathbf{D}$ is an arbitrary tensor function, while $\mathbf{d}_\mathrm{p}$ is an arbitrary tensor function that obeys Eq. (S-21), and using the non-negativity of the function Ξ, we conclude that inequality (S-45) is satisfied, provided that the Cauchy stress tensor $\mathbf{\Sigma}$ is given by

$$\begin{aligned}\mathbf{\Sigma} &= -\Pi\,\mathbf{I}+\frac{2}{1+Q}\biggl\{\Bigl[W_{\mathrm{e},1}\mathbf{B}_\mathrm{e}-W_{\mathrm{e},2}I_{\mathrm{e}3}\mathbf{B}_\mathrm{e}^{-1}+\Bigl(W_{\mathrm{e},2}I_{\mathrm{e}2}+W_{\mathrm{e},3}I_{\mathrm{e}3}\Bigr)\mathbf{I}\Bigr]\\ &\quad+\int_0^\infty\biggl[n(t,0,u)\Bigl(w_{,1}\mathbf{b}_0-w_{,2}I_{03}\mathbf{b}_0^{-1}+\Bigl(w_{,2}I_{02}+w_{,3}I_{03}\Bigr)\mathbf{I}\Bigr)\\ &\quad+\int_0^t\frac{\partial n}{\partial\tau}(t,\tau,u)\Bigl(w_{,1}\mathbf{b}_\tau-w_{,2}I_{\tau3}\mathbf{b}_\tau^{-1}+\Bigl(w_{,2}I_{\tau2}+w_{,3}I_{\tau3}\Bigr)\mathbf{I}\Bigr)\mathrm{d}\tau\biggr]\mathrm{d}u\biggr\},\end{aligned}\tag{S-46}$$

and plastic deformation of the permanent network is governed by the equation

$$\mathbf{d}_\mathrm{p}=\mathcal{P}\biggl[\Bigl(W_{\mathrm{e},1}\mathbf{C}_\mathrm{e}-W_{\mathrm{e},2}\mathbf{C}_\mathrm{e}^{-1}\Bigr)-\Bigl(W_{\mathrm{p},1}\mathbf{b}_\mathrm{p}-W_{\mathrm{p},2}\mathbf{b}_\mathrm{p}^{-1}\Bigr)\biggr]',\tag{S-47}$$

where $\mathcal{P}$ is an arbitrary non-negative function. Eq. (S-47) is equivalent to the equation

$$\begin{aligned}\mathbf{d}_\mathrm{p} &= \mathcal{P}\biggl[\Bigl(W_{\mathrm{e},1}\mathbf{C}_\mathrm{e}-W_{\mathrm{e},2}\mathbf{C}_\mathrm{e}^{-1}\Bigr)-\Bigl(W_{\mathrm{p},1}\mathbf{b}_\mathrm{p}-W_{\mathrm{p},2}\mathbf{b}_\mathrm{p}^{-1}\Bigr)\\ &\quad-\frac{1}{3}\Bigl(\Bigl(W_{\mathrm{e},1}I_{\mathrm{e}1}-W_{\mathrm{e},2}I_{\mathrm{e}2}\Bigr)-\Bigl(W_{\mathrm{p},1}I_{\mathrm{p}1}-W_{\mathrm{p},2}I_{\mathrm{p}2}\Bigr)\Bigr)\mathbf{I}\biggr].\end{aligned}\tag{S-48}$$

Constitutive Eqs. (S-46) and (S-48) are accompanied by the equilibrium equation for the stress tensor

$$\boldsymbol{\nabla}\cdot\mathbf{\Sigma}=\mathbf{0}\tag{S-49}$$

and the corresponding initial and boundary conditions.

For definiteness, analogs of the neo–Hookean equation are adopted for the strain energy density of the permanent network, the energy density of plastic deformation, and the mechanical energy of active chains in the transient network

$$\begin{aligned}W_\mathrm{e} &= \frac{1}{2}G_\mathrm{e}\Bigl[(I_{\mathrm{e}1}-3)-\ln I_{\mathrm{e}3}\Bigr],\qquad W_\mathrm{p}=\frac{1}{2}G_\mathrm{p}(I_{\mathrm{p}1}-3),\\ w &= \frac{1}{2}g\Bigl[(I_{\tau1}-3)-\ln I_{\tau3}\Bigr]\qquad(\tau\geq0),\end{aligned}\tag{S-50}$$

where G_e, G_p and g are constant elastic moduli.

Insertion of Eq. (S-50) into Eq. (S-48) implies that

$$\mathbf{d}_\mathrm{p}=\frac{1}{2}\mathcal{P}G_\mathrm{e}\biggl[\Bigl(\mathbf{C}_\mathrm{e}-\frac{1}{3}I_{\mathrm{e}1}\mathbf{I}\Bigr)-\mathcal{R}\Bigl(\mathbf{b}_\mathrm{p}-\frac{1}{3}I_{\mathrm{p}1}\mathbf{I}\Bigr)\biggr],\tag{S-51}$$

where

$$\mathcal{R}=\frac{G_\mathrm{p}}{G_\mathrm{e}}.\tag{S-52}$$

Combination of Eqs. (S-15) and (S-51) results in the differential equation for the tensor $\mathbf{b}_\mathrm{p}$,

$$\dot{\mathbf{b}}_\mathrm{p}=\mathcal{P}G_\mathrm{e}\biggl[\frac{1}{2}\Bigl(\mathbf{C}_\mathrm{e}\cdot\mathbf{b}_\mathrm{p}+\mathbf{b}_\mathrm{p}\cdot\mathbf{C}_\mathrm{e}\Bigr)-\frac{1}{3}(I_{\mathrm{e}1}-\mathcal{R}I_{\mathrm{p}1})\mathbf{b}_\mathrm{p}-\mathcal{R}\mathbf{b}_\mathrm{p}^2\biggr].\tag{S-53}$$

Inserting expression (S-51) into Eq. (S-25), we arrive at the differential equation for the tensor $\mathbf{C}_\mathrm{e}$,

$$\dot{\mathbf{C}}_\mathrm{e} = 2\mathbf{F}_\mathrm{e}^\top \cdot \mathbf{D} \cdot \mathbf{F}_\mathrm{e} + \mathcal{P}G_\mathrm{e}\left[\frac{1}{2}\mathcal{R}\Big(\mathbf{C}_\mathrm{e}\cdot\mathbf{b}_\mathrm{p} + \mathbf{b}_\mathrm{p}\cdot\mathbf{C}_\mathrm{e}\Big) + \frac{1}{3}(I_{\mathrm{e}1} - \mathcal{R}I_{\mathrm{p}1})\mathbf{C}_\mathrm{e} - \mathbf{C}_\mathrm{e}^2\right]. \tag{S-54}$$

It follows from Eqs. (S-37), (S-38), (S-46) and (S-50) that the stress tensor reads

$$\begin{aligned}\boldsymbol{\Sigma} \;=\; & -\Pi\,\mathbf{I} + \frac{1}{1+Q}\Bigg\{G_\mathrm{e}(\mathbf{B}_\mathrm{e} - \mathbf{I}) + G_\mathrm{a}\int_0^\infty f(u)\Bigg[\exp\Big(-\int_0^t \Gamma(s,u)\mathrm{d}s\Big)\mathbf{b}_0 \\ & + \int_0^t \Gamma(\tau,u)\exp\Big(-\int_\tau^t \Gamma(s,u)\mathrm{d}s\Big)\mathbf{b}_\tau \mathrm{d}\tau - \mathbf{I}\Bigg]\mathrm{d}u\Bigg\}\end{aligned} \tag{S-55}$$

with

$$G_\mathrm{a} = gN_\mathrm{a}. \tag{S-56}$$

Applying Eqs. (S-26)–(S-28) and (S-33), we find from Eq. (S-55) that

$$\boldsymbol{\Sigma} = -\Pi\,\mathbf{I} + \frac{1}{1+Q}\Big[G_\mathrm{e}(\mathbf{B}_\mathrm{e} - \mathbf{I}) + G_\mathrm{a}(\mathbf{F}\cdot\mathbf{S}\cdot\mathbf{F}^\top - \mathbf{I})\Big], \tag{S-57}$$

where

$$\mathbf{S} = \int_0^\infty f(u)\mathbf{s}(t,u)\mathrm{d}u \tag{S-58}$$

with

$$\mathbf{s}(t,u) = \exp\Big(-\int_0^t \Gamma(s,u)\mathrm{d}s\Big)\mathbf{C}_\mathrm{r}^{-1} + \int_0^t \Gamma(\tau,u)\exp\Big(-\int_\tau^t \Gamma(s,u)\mathrm{d}s\Big)\mathbf{C}^{-1}(\tau)\mathrm{d}\tau. \tag{S-59}$$

Here

$$\mathbf{C} = \mathbf{F}\cdot\mathbf{F}^\top, \qquad \mathbf{C}_\mathrm{r} = \mathbf{F}_\mathrm{r}\cdot\mathbf{F}_\mathrm{r}^\top \tag{S-60}$$

are the right Cauchy–Green tensors for macro-deformation and for transition from the initial state into the as-prepared state, respectively.

Differentiation of Eq. (S-59) with respect to time implies that the tensor function $\mathbf{s}(t,u)$ obeys the equation

$$\frac{\partial \mathbf{s}}{\partial t}(t,u) = \Gamma(t,u)\Big(\mathbf{C}^{-1}(t) - \mathbf{s}(t,u)\Big) \tag{S-61}$$

with the initial condition

$$\mathbf{s}(0,u) = \mathbf{C}_\mathrm{r}^{-1}. \tag{S-62}$$

The time $t = 0$ in Eq. (S-61) corresponds to the instant when the permanent and transient networks are formed under preparation conditions. Deformation of a fully swollen gel (equilibrated before loading) starts at some instant $t_0 > 0$ such that

$$\Gamma t_0 \gg 1$$

for meso-domains with all activation energies u under consideration. Bearing in mind that

$$\mathbf{C} = (1+Q)^{\frac{2}{3}}\mathbf{I}$$

after swelling and before testing of a gel, we find from Eq. (S-61) that the function $\mathbf{s}$ tends to its limiting value $(1+Q)^{-\frac{2}{3}}\mathbf{I}$ during the equilibration period. Adopting this value as the initial condition for the function $\mathbf{s}$ under deformation, and introducing the new time $t^* = t - t_0$ (for simplicity, the asterisk is omitted in what follows), we arrive at the the stress–strain relation (S-57), where $\mathbf{S}$ is given by Eq. (S-58), and $\mathbf{s}$ obeys Eq. (S-61) with the initial condition

$$\mathbf{s}(0,u) = (1+Q)^{-\frac{2}{3}}\mathbf{I}. \tag{S-63}$$

4 Uniaxial tension

Under uniaxial tension, the deformation gradient for macro-deformation reads

$$\mathbf{F} = (1+Q)^{\frac{1}{3}}\Big[k\boldsymbol{i}_1\boldsymbol{i}_1 + \frac{1}{\sqrt{k}}(\boldsymbol{i}_2\boldsymbol{i}_2 + \boldsymbol{i}_3\boldsymbol{i}_3)\Big], \tag{S-64}$$

where k stands for elongation ratio, $k(0) = 1$, and $\boldsymbol{i}_m$ $(m = 1, 2, 3)$ are unit vectors of a Cartesian frame. Eqs. (S-5), (S-12) and (S-64) imply that

$$\mathbf{D} = \frac{\dot{k}}{k}\Big[\boldsymbol{i}_1\boldsymbol{i}_1 - \frac{1}{2}(\boldsymbol{i}_2\boldsymbol{i}_2 + \boldsymbol{i}_3\boldsymbol{i}_3)\Big]. \tag{S-65}$$

We search the deformation gradient for plastic deformation $\mathbf{F}_{\rm p}$ is the form similar to Eq. (S-64),

$$\mathbf{F}_{\rm p} = (1+Q_{\rm r})^{\frac{1}{3}}\Big[k_{\rm p}\boldsymbol{i}_1\boldsymbol{i}_1 + \frac{1}{\sqrt{k_{\rm p}}}(\boldsymbol{i}_2\boldsymbol{i}_2 + \boldsymbol{i}_3\boldsymbol{i}_3)\Big], \tag{S-66}$$

where the function $k_{\rm p}(t)$ obeys the initial condition $k_{\rm p}(0) = 1$ (this equality ensures that Eq. (S-3) is satisfied). Combination of Eqs. (S-7), (S-9) and (S-66) yields

$$\mathbf{d}_{\rm p} = \frac{\dot{k}_{\rm p}}{k_{\rm p}}\Big[\boldsymbol{i}_1\boldsymbol{i}_1 - \frac{1}{2}(\boldsymbol{i}_2\boldsymbol{i}_2 + \boldsymbol{i}_3\boldsymbol{i}_3)\Big]. \tag{S-67}$$

We suppose that the deformation gradient for elastic deformation is given by

$$\mathbf{F}_{\rm e} = k_{\rm e}\boldsymbol{i}_1\boldsymbol{i}_1 + \frac{1}{\sqrt{k_{\rm e}}}(\boldsymbol{i}_2\boldsymbol{i}_2 + \boldsymbol{i}_3\boldsymbol{i}_3), \tag{S-68}$$

where the unknown function $k_{\rm e}(t)$ obeys the initial condition $k_{\rm e}(0) = 1$. Substitution of expressions (S-66), (S-68) into Eqs. (S-14), (S-19), respectively, results in

$$\mathbf{b}_{\rm p} - \frac{1}{3}I_{\rm p1}\mathbf{I} = \frac{2}{3}(1+Q_{\rm r})^{\frac{2}{3}}\Big(k_{\rm p}^2 - \frac{1}{k_{\rm p}}\Big)\Big[\boldsymbol{i}_1\boldsymbol{i}_1 - \frac{1}{2}(\boldsymbol{i}_2\boldsymbol{i}_2 + \boldsymbol{i}_3\boldsymbol{i}_3)\Big],$$
$$\mathbf{C}_{\rm e} - \frac{1}{3}I_{\rm e1}\mathbf{I} = \frac{2}{3}\Big(k_{\rm e}^2 - \frac{1}{k_{\rm e}}\Big)\Big[\boldsymbol{i}_1\boldsymbol{i}_1 - \frac{1}{2}(\boldsymbol{i}_2\boldsymbol{i}_2 + \boldsymbol{i}_3\boldsymbol{i}_3)\Big].$$

Inserting these expressions and Eq. (S-67) into Eq. (S-51), we arrive at the differential equation

$$\frac{\dot{k}_\mathrm{p}}{k_\mathrm{p}} = P\Big(\frac{k_\mathrm{e}^3-1}{k_\mathrm{e}} - R\frac{k_\mathrm{p}^3-1}{k_\mathrm{p}}\Big), \tag{S-69}$$

where

$$P = \frac{1}{3}\mathcal{P}G_\mathrm{e}, \qquad R = \mathcal{R}(1+Q_\mathrm{r})^{\frac{2}{3}}.$$

Combination of Eqs. (S-19) and (S-68) yields

$$\dot{\mathbf{C}}_\mathrm{e} = 2\frac{\dot{k}_\mathrm{e}}{k_\mathrm{e}}\Big[k_\mathrm{e}^2\boldsymbol{i}_1\boldsymbol{i}_1 - \frac{1}{2k_\mathrm{e}}(\boldsymbol{i}_2\boldsymbol{i}_2+\boldsymbol{i}_3\boldsymbol{i}_3)\Big].$$

It follows from Eqs. (S-65) and (S-68) that

$$\mathbf{F}_\mathrm{e}^\top\cdot\mathbf{D}\cdot\mathbf{F}_\mathrm{e} = \frac{\dot{k}}{k}\Big[k_\mathrm{e}^2\boldsymbol{i}_1\boldsymbol{i}_1 - \frac{1}{2k_\mathrm{e}}(\boldsymbol{i}_2\boldsymbol{i}_2+\boldsymbol{i}_3\boldsymbol{i}_3)\Big].$$

Eqs. (S-14), (S-19), (S-66) and (S-68) imply that

$$\begin{aligned}&\frac{1}{2}\mathcal{R}\Big(\mathbf{C}_\mathrm{e}\cdot\mathbf{b}_\mathrm{p}+\mathbf{b}_\mathrm{p}\cdot\mathbf{C}_\mathrm{e}\Big)+\frac{1}{3}(I_{\mathrm{e}1}-\mathcal{R}I_{\mathrm{p}1})\mathbf{C}_\mathrm{e}-\mathbf{C}_\mathrm{e}^2\\ &=-\frac{2}{3}\Big(\frac{k_\mathrm{e}^3-1}{k_\mathrm{e}}-R\frac{k_\mathrm{p}^3-1}{k_\mathrm{p}}\Big)\Big[k_\mathrm{e}^2\boldsymbol{i}_1\boldsymbol{i}_1-\frac{1}{2k_\mathrm{e}}(\boldsymbol{i}_2\boldsymbol{i}_2+\boldsymbol{i}_3\boldsymbol{i}_3)\Big].\end{aligned}$$

Inserting these expressions into Eq. (S-54), we arrive at the equation

$$\frac{\dot{k}_\mathrm{e}}{k_\mathrm{e}} = \frac{\dot{k}}{k} - P\Big(\frac{k_\mathrm{e}^3-1}{k_\mathrm{e}} - R\frac{k_\mathrm{p}^3-1}{k_\mathrm{p}}\Big). \tag{S-70}$$

Combination of Eqs. (S-69) and (S-70) results in the kinematic relation

$$\frac{\dot{k}_\mathrm{e}}{k_\mathrm{e}} = \frac{\dot{k}}{k} - \frac{\dot{k}_\mathrm{p}}{k_\mathrm{p}}. \tag{S-71}$$

We search the tensor function $\mathbf{s}(t,u)$ in the form

$$\mathbf{s} = (1+Q)^{-\frac{2}{3}}\Big[s_1\boldsymbol{i}_1\boldsymbol{i}_1 + s_2(\boldsymbol{i}_2\boldsymbol{i}_2+\boldsymbol{i}_3\boldsymbol{i}_3)\Big], \tag{S-72}$$

where the functions $s_m(t,u)$ $(m=1,2)$ satisfy the condition $s_1(0,u)=s_2(0,u)=1$ (this equality follows from Eq. (S-63)). Keeping in mind that

$$\mathbf{C}^{-1} = (1+Q)^{-\frac{2}{3}}\Big[k^{-2}\boldsymbol{i}_1\boldsymbol{i}_1 + k(\boldsymbol{i}_2\boldsymbol{i}_2+\boldsymbol{i}_3\boldsymbol{i}_3)\Big],$$

and inserting Eq. (S-72) into Eq. (S-61), we arrive at the equations

$$\frac{\partial s_1}{\partial t} = \Gamma\Big(\frac{1}{k^2}-s_1\Big), \qquad \frac{\partial s_2}{\partial t} = \Gamma(k-s_2). \tag{S-73}$$

It follows from Eqs. (S-58) and (S-72) that

$$\mathbf{S} = (1+Q)^{-\frac{2}{3}}\Big[S_1\boldsymbol{i}_1\boldsymbol{i}_1 + S_2(\boldsymbol{i}_2\boldsymbol{i}_2+\boldsymbol{i}_3\boldsymbol{i}_3)\Big], \tag{S-74}$$

where

$$S_1 = \int_0^\infty f(u)s_1(t,u)\mathrm{d}u, \qquad S_2 = \int_0^\infty f(u)s_2(t,u)\mathrm{d}u. \tag{S-75}$$

Substitution of Eqs. (S-64), (S-68) and (S-74) into Eq. (S-57) implies that the Cauchy stress tensor $\boldsymbol{\Sigma}$ reads

$$\boldsymbol{\Sigma} = \Sigma_1 \boldsymbol{i}_1\boldsymbol{i}_1 + \Sigma_2(\boldsymbol{i}_2\boldsymbol{i}_2 + \boldsymbol{i}_3\boldsymbol{i}_3), \tag{S-76}$$

where

$$\begin{aligned}
\Sigma_1 &= -\Pi + \frac{1}{1+Q}\Big[G_{\mathrm{e}}(k_{\mathrm{e}}^2 - 1) + G_{\mathrm{a}}\Big((1+Q)^{-\frac{2}{3}}S_1k^2 - 1\Big)\Big],\\
\Sigma_2 &= -\Pi + \frac{1}{1+Q}\Big[G_{\mathrm{e}}\Big(\frac{1}{k_{\mathrm{e}}} - 1\Big) + G_{\mathrm{a}}\Big((1+Q)^{-\frac{2}{3}}\frac{S_2}{k} - 1\Big)\Big].
\end{aligned}$$

It follows from the equilibrium equation and the boundary condition in stresses at the lateral surface of a sample that

$$\Sigma_2 = 0.$$

Combination of these equalities implies that

$$\Sigma_1 = \frac{1}{1+Q}\Big[G_{\mathrm{e}}\Big(k_{\mathrm{e}}^2 - \frac{1}{k_{\mathrm{e}}}\Big) + G_{\mathrm{a}}(1+Q)^{-\frac{2}{3}}\Big(S_1k^2 - \frac{S_2}{k}\Big)\Big]. \tag{S-77}$$

Introducing the engineering tensile stress

$$\sigma = \frac{\Sigma_1}{k},$$

we find from Eq. (S-77) that

$$\sigma = G\Big[(1-\kappa)\frac{k_{\mathrm{e}}^3 - 1}{kk_{\mathrm{e}}} + \kappa\Big(S_1k - \frac{S_2}{k^2}\Big)\Big], \tag{S-78}$$

where

$$G = \frac{1}{1+Q}\Big[G_{\mathrm{e}} + \frac{G_{\mathrm{a}}}{(1+Q)^{\frac{2}{3}}}\Big], \qquad \kappa = \frac{G_{\mathrm{a}}}{G_{\mathrm{a}} + G_{\mathrm{e}}(1+Q)^{\frac{2}{3}}}. \tag{S-79}$$

Eqs. (S-69), (S-71), (S-73), (S-75) and (S-78) provide a set of governing equations for uniaxial tension with an arbitrary deformation program $k(t)$. To simplify these relations, we integrate Eq. (S-71) from $t = 0$ to an arbitrary instant $t > 0$ and obtain

$$\ln\frac{k_{\mathrm{e}}}{k_{\mathrm{e}}(0)} = \ln\frac{k}{k(0)} - \ln\frac{k_{\mathrm{p}}}{k_{\mathrm{p}}(0)}. \tag{S-80}$$

Bearing in mind that $k(0) = 1$, $k_{\mathrm{e}}(0) = 1$ and $k_{\mathrm{p}}(0) = 1$, we find from Eq. (S-80) that

$$k_{\mathrm{e}} = \frac{k}{k_{\mathrm{p}}}. \tag{S-81}$$

Insertion of expression (S-81) into the stress–strain relation (S-78) implies that

$$\sigma = G\Big[(1-\kappa)\frac{k^3-k_\mathrm{p}^3}{k^2k_\mathrm{p}^2} + \kappa\Big(S_1k - \frac{S_2}{k^2}\Big)\Big], \tag{S-82}$$

Combination of Eqs. (S-69) and (S-81) results in the kinetic equation for plastic deformation

$$\dot{k}_\mathrm{p} = P\Big[\frac{k^3-k_\mathrm{p}^3}{kk_\mathrm{p}} - R(k_\mathrm{p}^3-1)\Big]. \tag{S-83}$$

Under stretching and retraction with a constant strain rate $\dot{\epsilon}$, Eqs. (S-73), (S-75), (S-82), (S-83) are solved together with an additional kinematic relation

$$\dot{k} = \pm\dot{\epsilon}, \tag{S-84}$$

where the signs "+" and "–" correspond to loading and unloading, respectively.

5 Kinetics of self-recovery

We analyze recovery of a gel specimen subjected to uniaxial stretching up to maximum elongation ratio k_max and retraction down to the zero stress. Recovery starts at some instant t_0 when tensile stress σ vanishes, elongation ratio for macro-deformation equals k_0, and elongation ratio for plastic deformation equals k_p0.

Keeping in mind that $\sigma(t) = 0$ under recovery, we find from Eq. (S-82) that

$$(1-\kappa)\frac{k^3-k_\mathrm{p}^3}{k^2k_\mathrm{p}^2} + \kappa\Big(S_1k - \frac{S_2}{k^2}\Big) = 0. \tag{S-85}$$

Resolving Eq. (S-85) with respect to k, we conclude that

$$k = \left(\frac{k_\mathrm{p}+\kappa_1S_2}{k_\mathrm{p}^{-2}+\kappa_1S_1}\right)^{\frac{1}{3}}, \tag{S-86}$$

where

$$\kappa_1 = \frac{\kappa}{1-\kappa}. \tag{S-87}$$

Combining Eqs. (S-83) and (S-85), we arrive at the governing equation for plastic deformation under recovery

$$\dot{k}_\mathrm{p} = -P\Big[\kappa_1k_\mathrm{p}\Big(S_1k^2 - \frac{S_2}{k}\Big) + R(k_\mathrm{p}^3-1)\Big] \tag{S-88}$$

with the initial condition $k_\mathrm{p}(t_0) = k_\mathrm{p0}$.

Eqs. (S-73), (S-75), (S-86) and (S-88) provide kinetic equations for self-recovery of a DN gel.

Tables

Table S1: Total recovery of DN gels subjected to cyclic deformation with various maximum elongation ratios $k_{\max}$

Duration	$k_{\max}$	Reference
2 min	9.0	[1]
5 min	9.0	[2]
10 min	4.0	[3]
15 min	5.0	[4]
1 h	4.0	[5]
2 h	4.0	[6]
4 h	2.5	[7]
4 h	3.5	[8]
4 h	4.0	[9]
12 h	11.0	[10]
1 day	7.0	[11]
30 h	11.0	[12]

References

[1] J. Liu, C.S.Y. Tan, Z. Yu, Y. Lan, C. Abell, O.A. Scherman, *Adv. Mater.* **2017**, *29*, 1604951.

[2] H. Fan, J. Wang, Z. Jin, *Macromolecules* **2018**, *51*, 1696.

[3] H. Ding, X.N. Zhang, S.Y. Zheng, Y. Song, Z.L. Wu, Q. Zheng, *Polymer* **2017**, *131*, 95.

[4] M.A. Haque, T. Kurokawa, G. Kamita, J.P. Gong, *Macromolecules* **2011**, *44*, 8916.

[5] X. Hu, M. Vatankhah-Varnoosfaderani, J. Zhou, Q. Li, S.S. Sheiko, *Adv. Mater.* **2015**, *27*, 6899.

[6] T.L. Sun, T. Kurokawa, S. Kuroda, A.B. Ihsan, T. Akasaki, K. Sato, M.A. Haque, T. Nakajima, J.P. Gong, *Nat. Mater.* **2013**, *12*, 932.

[7] K. Peng, H. Yu, H. Yang, X. Hao, A. Yasin, X. Zhang, *Soft Matter* **2017**, *13*, 2135.

[8] S.Y. Zheng, H. Ding, J. Qian, J. Yin, Z.L. Wu, Y. Song, Q. Zheng, *Macromolecules* **2016**, *49*, 9637.

[9] P. Lin, S. Ma, X. Wang, F. Zhou, *Adv. Mater.* **2015**, *27*, 2054.

[10] M. Zhong, Y.-T. Liu, X.-Y. Liu, F.-K. Shi, L.-Q. Zhang, M.-F. Zhu, X.-M. Xie, *Soft Matter* **2016**, *12*, 5420.

[11] J.-Y. Sun, X. Zhao, W.R.K. Illeperuma, O. Chaudhuri, K.H. Oh, D.J. Mooney, J.J. Vlassak, Z. Suo, *Nature* **2012**, *489*, 133.

[12] Y. Sun, G. Gao, G. Du, Y. Cheng, J. Fu, *ACS Macro Lett.* **2014**, *3*, 496.

Table S2: Material parameters for PVA gel (Fig. 1)

Parameter	Value
G (kPa)	22.5
κ	0.865
γ (s^{-1})	3.5
Σ	2.4

Table S3: Material parameters for MAAc-VP-PEGMA gel (Fig. 2)

Parameter	Fig.2A	Fig. 2B
G (MPa)	0.8	0.68
κ	0.68	0.63
γ (s^{-1})	0.7	1.2
Σ	0.2	0.2
β_1 (MPa^{-1})	0.0	0.0
α	0.0	1.4
p_2 (s^{-1})	0.06	0.06
R_2	0.15	0.15
β_2	14.0	1.4
p_3 (s^{-1})	$2.0 \cdot 10^{-7}$	
R_3	$1.2 \cdot 10^{4}$	
$\bar{\sigma}$ (MPa)	0.0	

Table S4: Material parameters for AAm-AAc gel (Fig. 3)

Parameter	Value
G (MPa)	5.9
κ	0.72
γ (s^{-1})	0.25
Σ	0.75
p_1 (s^{-1})	0.038
R_1	0.35
β_1 (MPa^{-1})	0.18
α	-0.5
p_2 (s^{-1})	0.178
R_2	0.014
β_2	9.8
p_3 (s^{-1})	$3.0 \cdot 10^{-6}$
R_3	$2.8 \cdot 10^{3}$
$\bar{\sigma}$ (MPa)	1.4

Table S5: Material parameters for AAm-AAc-ODA gel (Fig. 4)

Parameter	Value
G (MPa)	2.63
κ	0.753
γ (s^{-1})	0.35
Σ	0.6
p_1 (s^{-1})	0.029
R_1	1.8
β_1 (MPa^{-1})	0.08
α	-3.6
p_2 (s^{-1})	0.0345
R_2	0.01
β_2	50.0
p_3 (s^{-1})	$7.0 \cdot 10^{-7}$
R_3	$2.8 \cdot 10^{3}$
$\bar{\sigma}$ (MPa)	0.2

Table S6: Material parameters for double cross-linked AAm-AAc gel (Fig. 5)

Parameter	Fig. 5A	Fig. 5B
G (MPa)	1.37	1.54
κ	0.53	0.62
γ (s^{-1})	0.06	0.06
Σ	0.3	0.3
p_1 (s^{-1})		0.015
R_1	0.18	0.35
β_1 (MPa^{-1})	0.45	0.6
α	-0.3	-0.8
p_2 (s^{-1})		0.113
R_2		0.043
β_2		8.0
p_3 (s^{-1})		$4.0 \cdot 10^{-7}$
R_3		$2.8 \cdot 10^{3}$
$\bar{\sigma}$ (MPa)		0.15

Table S7: Material parameters for PDMS-$FeCl_2$ elastomer (Fig. 6)

Parameter	Value
G (MPa)	0.34
κ	0.445
γ (s^{-1})	0.53
Σ	6.0

Figures

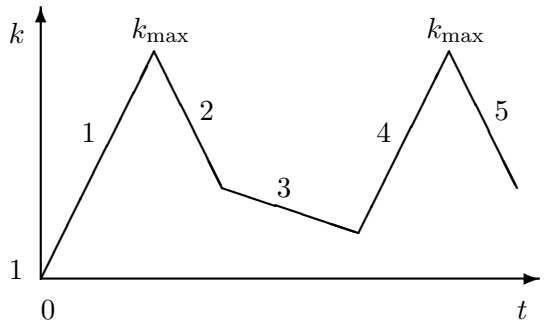

Figure S-1: Elongation ratio k versus time t in recovery test. 1: First stretching; 2: First retraction; 3: Recovery under the zero stress; 4: Second stretching; 5: Second retraction.

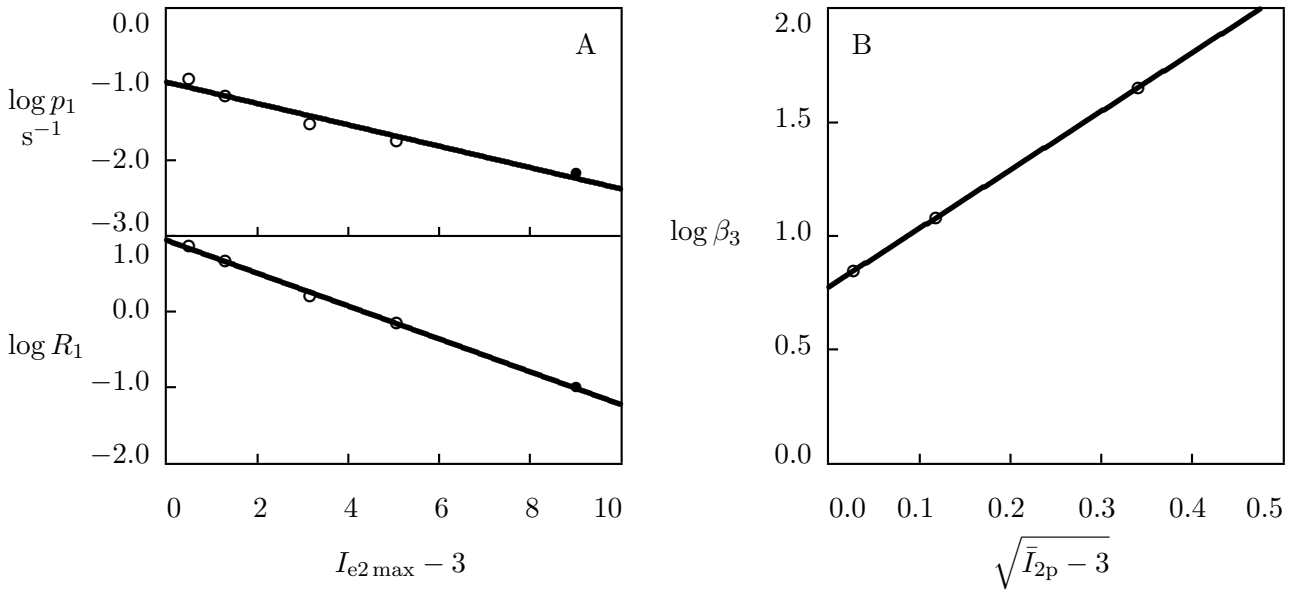

Figure S-2: A: Parameters p_1 and R_1 versus I_{e2} calculated at maximum elongation ratio k_{max}. Symbols: treatment of observations on MAAc-VP-PEGMA gel in cyclic tests with various k_{max} (Figs. 2A and 2B). Unfilled circles: Fig. 2A. Filled circles: Fig. 2B. Solid lines: approximation of the data by Eq. (16). B: Parameter β_3 versus I_{2p} calculated at the point with $\sigma = \bar{\sigma}$. Circles: treatment of observations in recovery tests with various durations of recovery (Fig. 2C). Solid line: approximation of the data by Eq. (17).

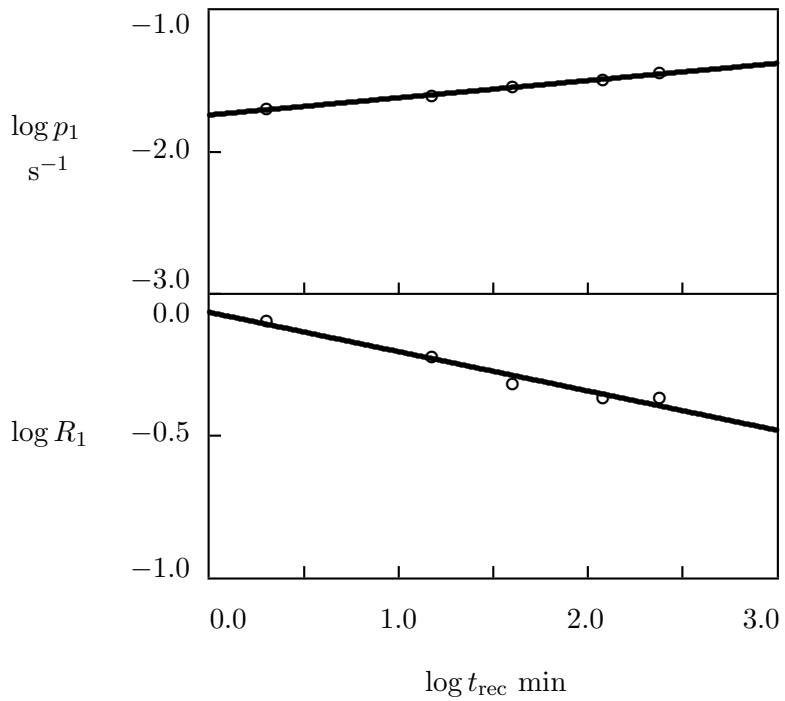

Figure S-3: Parameters p_1 and R_1 versus recovery time t_{rec}. Circles: treatment of observations on physically bonded AAm-AAc gel in recovery tests under the second retraction (Fig. 3A). Solid lines: approximation of the data by Eq. (18).

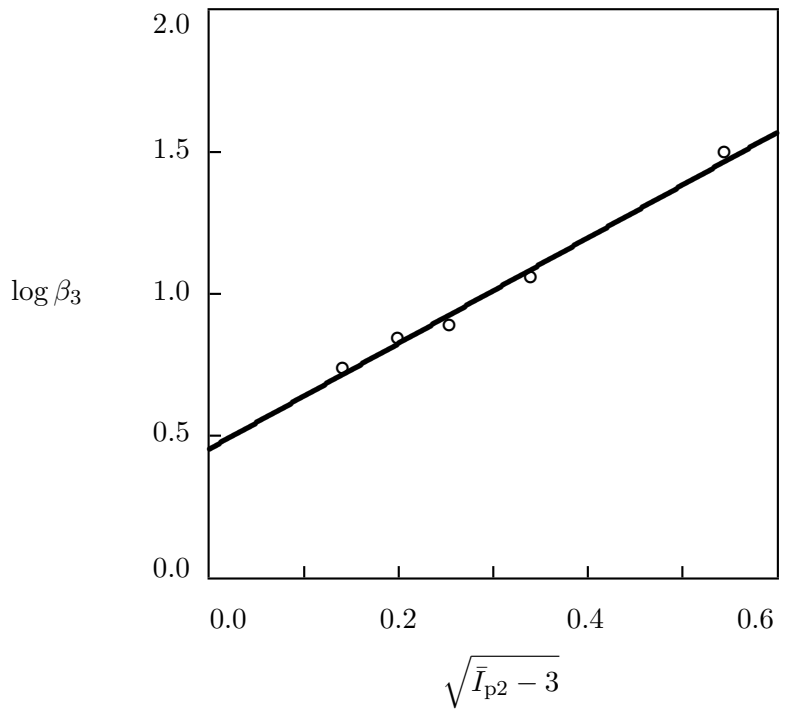

Figure S-4: Parameter β_3 versus $I_{2\mathrm{p}}$ calculated at the point with $\sigma = \bar{\sigma}$. Circles: treatment of observations on AAm-AAc-ODA gel in recovery tests with various durations of recovery (Fig. 4A). Solid line: approximation of the data by Eq. (17).

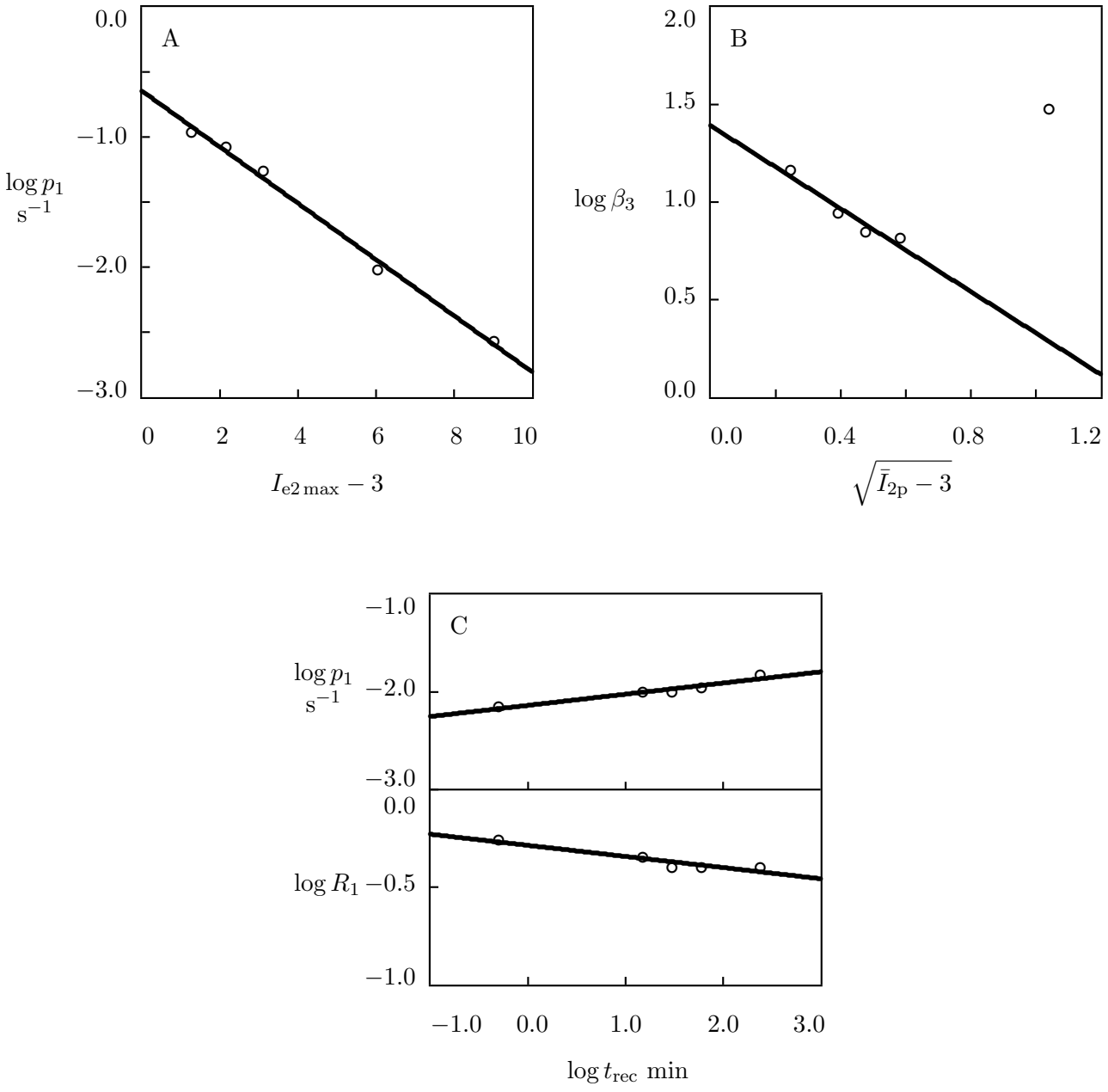

Figure S-5: A: Parameter p_1 versus I_{e2} calculated at maximum elongation ratio k_{max}. Circles: treatment of observations on double cross-linked AAm-AAc gel in cyclic tests with various k_{max} (Fig. 5A). Solid line: approximation of the data by Eq. (16). B: Parameter β_3 versus I_{2p} calculated at the point with $\sigma = \bar{\sigma}$. Circles: treatment of observations in recovery tests with various durations of recovery (Fig. 5B). Solid line: approximation of the data by Eq. (17). C: Parameters p_1 and R_1 versus recovery time t_{rec}. Circles: treatment of observations in recovery tests under the second retraction (Fig. 5B). Solid lines: approximation of the data by Eq. (18).

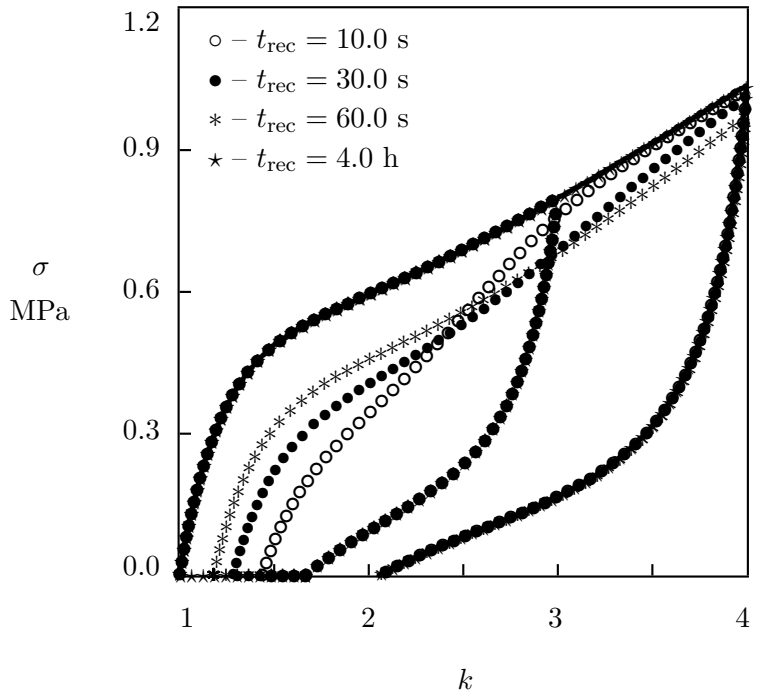

Figure S-6: Tensile stress σ versus elongation ratio k. Solid line: results of simulation for cyclic test on MAAc-VP-PEGMA gel with strain rate $\dot{\epsilon} = 0.154\ \mathrm{s}^{-1}$ and maximum elongation ratio $k_{\max} = 4$. Symbols: predictions of the model for multi-cycle tests that involve stretching up to $k_{\max 1} = 3$, retraction down to the zero stress, recovery for various times $t_{\rm rec}$, stretching up to $k_{\max 2} = 4$, and retraction down to the zero stress.

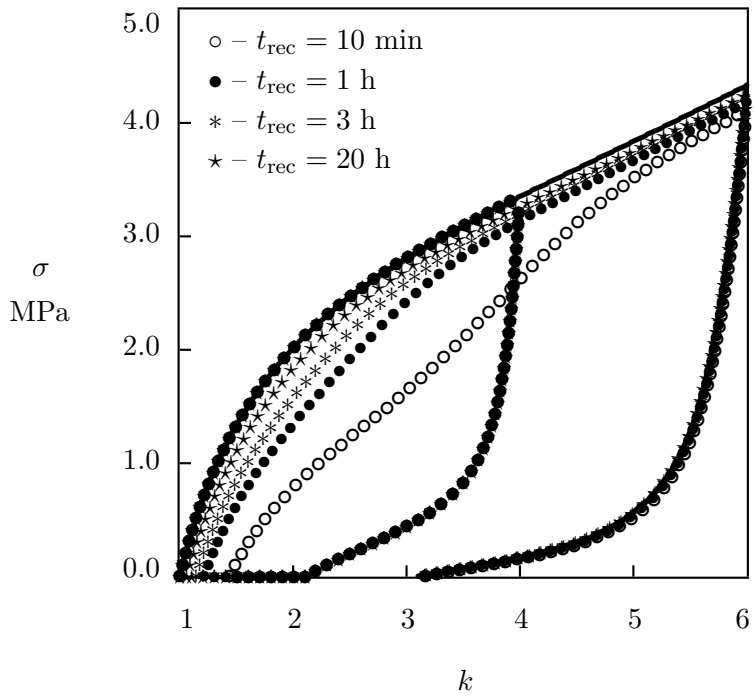

Figure S-7: Tensile stress σ versus elongation ratio k. Solid line: results of simulation for cyclic test on double cross-linked AAm–AAc gel with strain rate $\dot{\epsilon} = 0.083$ s^{-1} and maximum elongation ratio $k_{\max} = 6$. Symbols: predictions of the model for multi-cycle tests that involve stretching up to $k_{\max 1} = 4$, retraction down to the zero stress, recovery for various times $t_{\rm rec}$, stretching up to $k_{\max 2} = 6$, and retraction down to the zero stress.

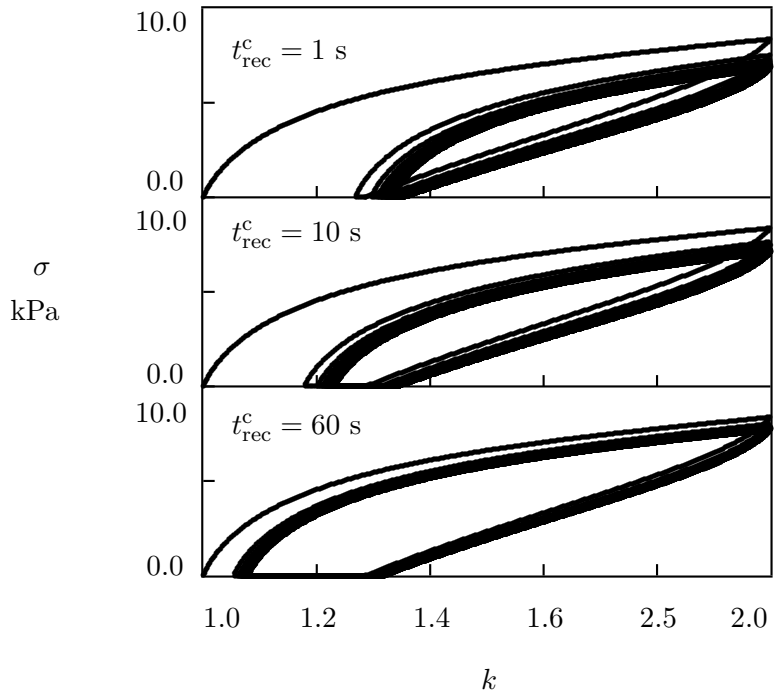

Figure S-8: Tensile stress σ versus elongation ratio k. Solid lines: predictions of the model for multi-cycle tests on PVA gel with strain rate $\dot{\epsilon} = 0.03$ s^{-1}, maximum elongation ratio per cycle $k_{\max} = 2$, and various recovery times between cycles $t_{\mathrm{rec}}^{\mathrm{c}}$.

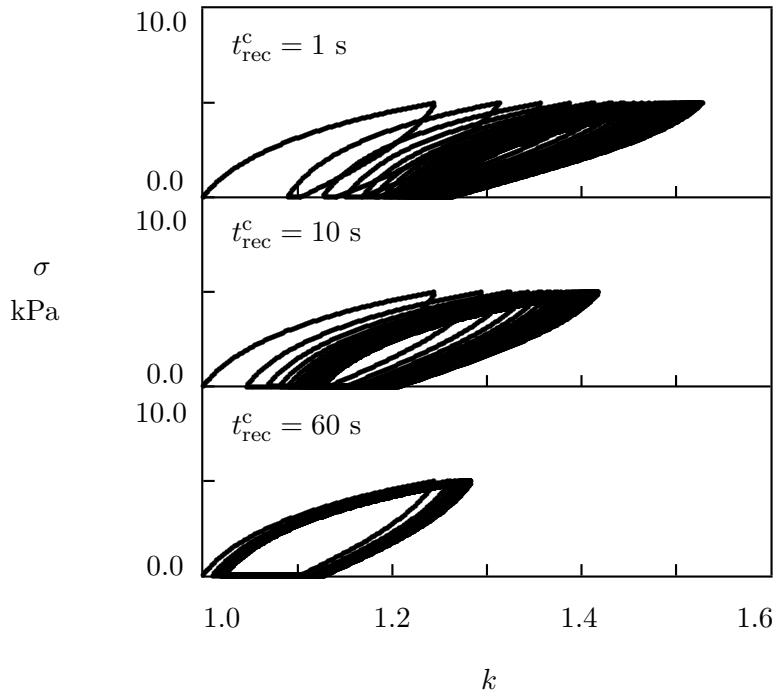

Figure S-9: Tensile stress σ versus elongation ratio k. Solid lines: predictions of the model for multi-cycle tests on PVA gel with strain rate $\dot{\epsilon} = 0.03$ s^{-1}, maximum stress per cycle $\sigma_{\mathrm{max}} = 5$ kPa, and various recovery times between cycles $t_{\mathrm{rec}}^{\mathrm{c}}$.

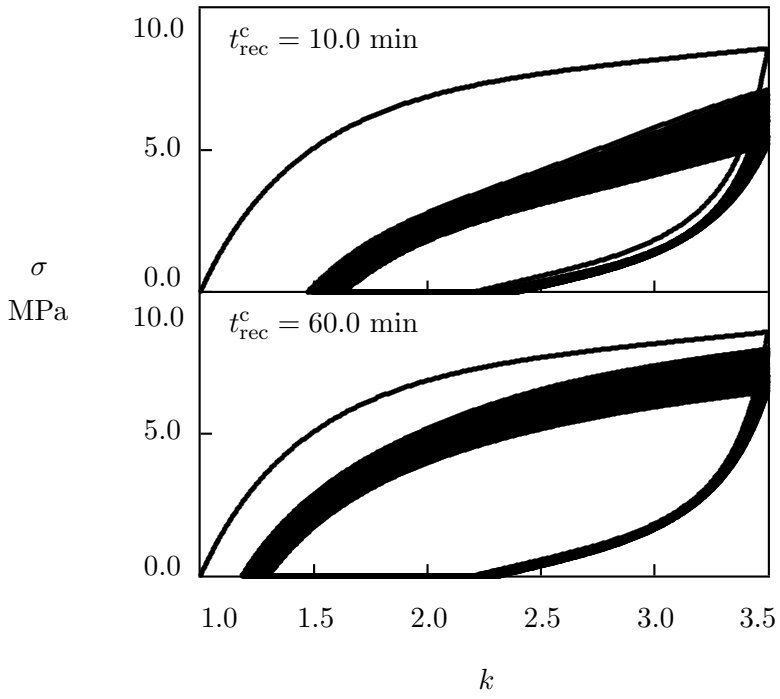

Figure S-10: Tensile stress σ versus elongation ratio k. Solid lines: predictions of the model for multi-cycle tests on AAm-AAc gel with strain rate $\dot{\epsilon} = 0.139$ s^{-1}, maximum elongation ratio $k_{max} = 3.5$, and various recovery times between cycles t^{c}_{rec}.